Mon. Not. R. Astron. Soc. **360,** 869–891 (2005) doi:10.1111/j.1365-2966.2005.08954.x

Polarization and structure of relativistic parsec-scale AGN jets

M. Lyutikov,[1,2,3]★ V. I. Pariev[4,5]† and D. C. Gabuzda[6]

[1]*Physics Department, McGill University, 3600 rue University, Montreal, QC, Canada H3A 2T8*
[2]*Canadian Institute for Theoretical Astrophysics, 60 St George, Toronto, Ont, M5S 3H8, Canada*
[3]*Kavli Institute for Particle Astrophysics and Cosmology, 2575 Sandhill Road, Menlo Park, CA 94305, USA*
[4]*Department of Physics and Astronomy, University of Rochester, Rochester, NY 14627, USA*
[5]*Lebedev Physical Institute, Leninsky Prospect 53, Moscow 119991, Russia*
[6]*Department of Physics, University College Cork, Cork, Ireland*

Accepted 2005 February 22. Received 2005 February 11; in original form 2004 June 6

ABSTRACT

We consider the polarization properties of optically thin synchrotron radiation emitted by relativistically moving electron–positron jets carrying large-scale helical magnetic fields. In our model, the jet is cylindrical and the emitting plasma moves parallel to the jet axis with a characteristic Lorentz factor Γ. We draw attention to the strong influence that the bulk relativistic motion of the emitting relativistic particles has on the observed polarization.

Our computations predict and explain the following behaviour. (i) For jets unresolved in the direction perpendicular to their direction of propagation, the position angle of the electric vector of the linear polarization has a bimodal distribution, being oriented either parallel or perpendicular to the jet. (ii) If an ultra-relativistic jet with $\Gamma \gg 1$ whose axis makes a small angle to the line of sight, $\theta \sim 1/\Gamma$, experiences a relatively small change in the direction of propagation, velocity or pitch angle of the magnetic fields, the polarization is likely to remain parallel or perpendicular; on the other hand, in some cases, the degree of polarization can exhibit large variations and the polarization position angle can experience abrupt 90° changes. This change is more likely to occur in jets with flatter spectra. (iii) In order for the jet polarization to be oriented along the jet axis, the intrinsic toroidal magnetic field (in the frame of the jet) should be of the order of or stronger than the intrinsic poloidal field; in this case, the highly relativistic motion of the jet implies that, in the observer's frame, the jet is strongly dominated by the toroidal magnetic field $B_\phi/B_z \geqslant \Gamma$. (iv) The emission-weighted average pitch angle of the intrinsic helical field in the jet must not be too small to produce polarization along the jet axis. In force-free jets with a smooth distribution of emissivities, the emission should be generated in a limited range of radii not too close to the jet core. (v) For mildly relativistic jets, when a counter-jet can be seen, the polarization of the counter-jet is preferentially orthogonal to the axis, unless the jet is strongly dominated by the toroidal magnetic field in its rest frame. (vi) For resolved jets, the polarization pattern is not symmetric with respect to jet axis. Under certain conditions, this can be used to deduce the direction of the spin of the central object (black hole or disc), whether it is aligned or anti-aligned with the jet axis. (vii) In resolved 'cylindrical shell' type jets, the central parts of the jet are polarized along the axis, while the outer parts are polarized orthogonal to it, in accordance with observations.

We conclude that large-scale magnetic fields can explain the salient polarization properties of parsec-scale AGN jets. Since the typical degrees of polarization are $\leqslant$15 per cent, the emitting parts of the jets must have comparable rest-frame toroidal and poloidal fields. In this case, most relativistic jets are strongly dominated by the toroidal magnetic field component in the observer's frame, $B_\phi/B_z \sim \Gamma$. We also discuss the possibility that relativistic AGN jets

★E-mail: lyutikov@physics.mcgill.ca
†Currently at: Physics Department, University of Wisconsin-Madison, 1150 University Ave., Madison, WI 53706, USA.

may be electromagnetically (Poynting flux) dominated. In this case, dissipation of the toroidal magnetic field (and not fluid shocks) may be responsible for particle acceleration.

Key words: MHD – radiation mechanisms: non-thermal – galaxies: active – galaxies: jets – galaxies: nuclei.

1 INTRODUCTION

VLBI linear polarization studies of compact parsec-scale jets in radio-loud AGNs have revealed a number of general tendencies (e.g. Cawthorne et al. 1993; Gabuzda, Pushkarev & Cawthorne 2000; Gabuzda 2003, and references therein). These tendencies include: (i) a roughly bimodal distribution of the electric vector position angles (EVPAs) for the jet linear polarization with respect to jet direction, with quasars tending to have polarization orthogonal to the jet and BL Lac objects tending to have polarization along the jet (Marscher et al. 2002); (ii) the EVPAs sometimes 'follow' the jet as it bends, keeping its relative orientation with respect to the jet direction (Fig. 1; see also Owen, Hardee & Cornwell 1989 for the kiloparsec jet in M87); (iii) the jet EVPAs sometimes experience orthogonal jumps along the jet, changing from aligned to orthogonal or vice versa (Gabuzda & Gómez 2001; Pushkarev et al. 2005; Fig. 2); (iv) in some resolved jets, the EVPA in the central part of the jet lies along the jet, while the edges are polarized orthogonally to the jet direction (Attridge, Roberts & Wardle 1999; Moellenbrock, Roberts & Wardle 2000; Pushkarev et al. 2005); (v) Faraday-rotation gradients are frequently observed across the jets of BL Lac objects (Gabuzda, Murray & Cronin 2004). All of these properties are statistical, each having a number of known exceptions.

The large-scale magnetic fields are almost universally accepted to play an important role in the production (e.g. Blandford & Znajek 1977), acceleration (e.g. Blandford & Payne 1982; Contopoulos & Lovelace 1994; Camenzind 1995) and, especially, collimation of the jets (e.g. Heyvaerts & Norman 1989; Sauty, Tsinganos & Trussoni 2002; Heyvaerts & Norman 2003); see also the review by Begelman, Blandford & Rees (1984). Yet their importance for jet propagation and emission generation is underestimated. Most commonly, polarization structure is attributed to transverse or oblique relativistic shocks propagating in the jet and compressing the upstream turbulent magnetic field, so that the compressed downstream magnetic field becomes anisotropically distributed (e.g. Laing 1980; Hughes, Aller & Aller 1989a,b). This mechanism produces fields compressed in the plane of the shock and is expected to produce polarization along the jet for the case of a transverse shock. Numerous observations of polarization orthogonal to the jet are attributed to a sheared component of magnetic field in a sheath surrounding the jet. This overall scenario is open to criticism. First, it is hard to see how weaker bridges with the same characteristic polarization connecting bright knots could be produced: this would require a quasi-steady sequence of weak shocks. Secondly, since internal shocks can be oblique, with a range of orientations, it is not natural to have a bimodal distribution of the relative EVPAs (the EVPAs in BL Lac seem to be in disagreement with the shock model Denn, Mutel & Marscher 2000). Thirdly, some features showing longitudinal polarization are far from being compact (e.g. the resolved VLBI jets of 1219+285, see Gabuzda et al. 1994, and 1803+784, see Gabuzda & Chernetskii 2003).

An alternative interpretation of the jet polarization, which we favour, is that the flow carries large-scale helical magnetic fields. In this paper, we calculate the polarization properties of a relativistic jet carrying helical magnetic fields and compare them with observations. The

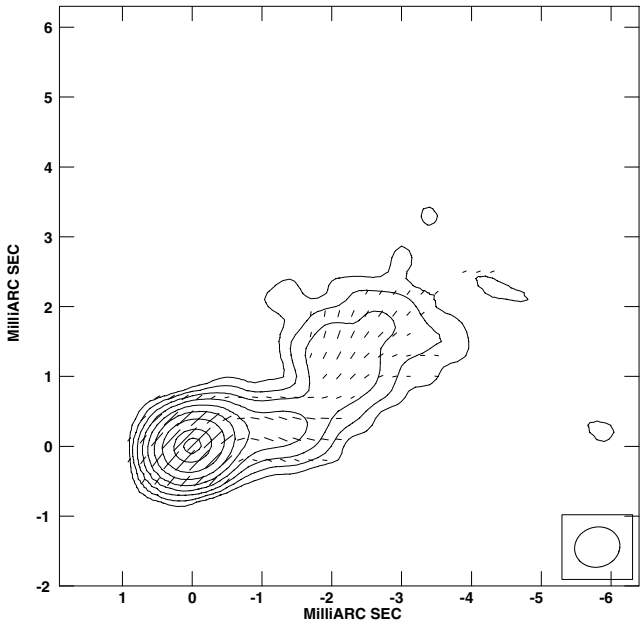

Figure 1. Observed 4-cm total-intensity contours and superposed linear-polarization vectors for the BL Lac object 1749+701: the polarization remains aligned with the jet direction as the jet bends (data processing is described in Gabuzda, Pushkarev & Garnich 2001a).

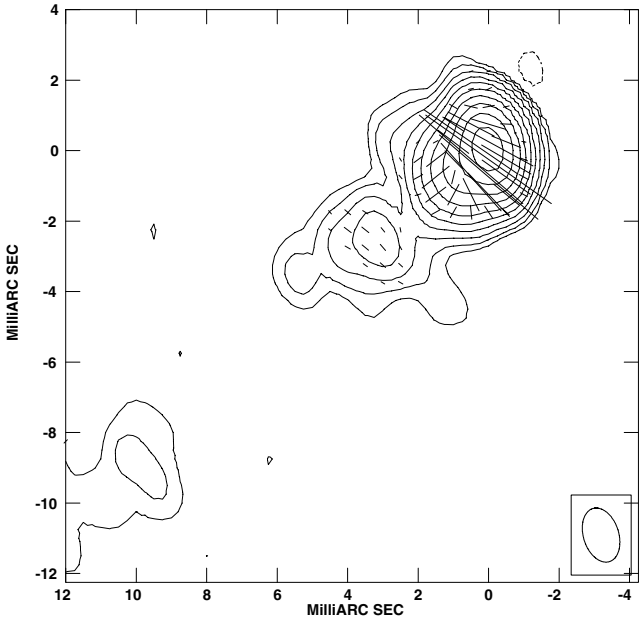

Figure 2. Observed 6-cm total-intensity contours and superposed linear-polarization vectors for the BL Lac object 1418+546: the orientation of the polarization relative to the jet displays jumps between being aligned with and orthogonal to the jet (data processing and further analysis are discussed in Pushkarev et al. (2005).

results are encouraging. We can both reproduce the average properties of the jet polarization, such as the bimodal distribution of the observed EVPAs, as well as allow for possible exceptions, such as orthogonal jumps in the EVPA along the jet.

There have been two approaches to studies of the synchrotron polarization of AGN jets. On the one hand, Laing (1980, 1981) developed detailed models for optically thin synchrotron emission from *non-relativistic jets*. Recently, such non-relativistic models were generalized to include plasma effects on the propagation of the radiation inside the jet, Faraday rotation and the Cotton–Mouton effect (Zheleznyakov & Koryagin 2002; Beckert & Falcke 2002; Beckert 2003; Ruszkowski 2003). In these works, although plasma is relativistic, the radiation and polarization transport are considered in a static medium. In actual jets, the plasma is in a state of bulk motion with relativistic speeds. On the other hand, the polarization properties of the synchrotron emission from relativistic AGN jets have been discussed by Blandford & Königl (1979), Bjornsson (1982) and Konigl & Choudhuri (1985), but not in the context of large-scale spiral magnetic fields. Pariev, Istomin & Beresnyak (2003) have investigated the polarization properties of a specific configuration of a spiral magnetic field with a uniform axial field, zero total poloidal current in the jet, and with sheared relativistic spiral motion of the plasma perpendicular to the magnetic field lines. In this paper, we present the results of fully relativistic calculations for various jet internal structures and the resulting polarization structures. We take a step back and try to answer the question of whether we can reproduce the most salient polarization features of AGN jets under generic assumptions about the internal helical magnetic field in the jet (basically generalizing the work of Laing 1981, to relativistic jets). In order to answer this question, one must know the internal structure of the jet (distribution of poloidal and toroidal magnetic fields) and the distribution of synchrotron emissivities. These are highly uncertain in terms of theoretical principles, and are also subject to averaging over the whole jet (for unresolved jets) and along the line of sight (for resolved jets).

Conventionally (and erroneously for a relativistically moving plasma!), the direction of the observed polarization for optically thin regions and the associated magnetic fields are assumed to be in one-to-one correspondence, being orthogonal to each other, so that some observers chose to plot the direction of the electric vector of the wave, while others plot vectors orthogonal to the electric vectors and call them the direction of the magnetic field. *This is correct only for non-relativistically moving sources, and thus cannot be applied to AGN jets.* First, relativistic boosting changes the relative strength of the magnetic field components along and orthogonal to the line of sight, which transform differently under the Lorentz boost. Thus, if we could see the magnetic fields directly, the strength of the jet poloidal and toroidal fields measured in the laboratory frame would be different from those measured in the jet frame. Secondly, since the emission is boosted by the relativistic motion of the jet material, the polarization EVPA rotates parallel to the plane containing the velocity vector of the emitting volume $\boldsymbol{v}$ and the unit vector in the direction to the observer $\hat{\boldsymbol{n}}$, so that *the observed electric field of the wave is not, in general, orthogonal to the observed magnetic field* (Blandford & Königl 1979; Lyutikov, Pariev & Blandford 2003). Thus, to reconstruct the internal structure of relativistic jets from polarization observations one needs to know both the polarization *and* the velocity field of the jet. Overall, plotting the direction of the electric field (EVPA) should be considered the only acceptable way to represent polarization data for sources where relativistic motion may be involved.

Because of the finite resolution of real polarimetric observations, the observed intensities of the polarized and unpolarized components are averages over the effective beam size. When the resolution is relatively low, the transverse distribution of the intensity is unresolved. In this case, only the intensity and polarization averaged over the jet size is observed. If the jet is circular in cross section and the distributions of the

magnetic fields, emitting particles and velocity fields are axisymmetric across the jet, then the whole jet can be decomposed into a collection of infinitesimally thin shells. These shells have constant components of the spiral magnetic field and constant emissivity along their perimeter, and are moving uniformly with a constant velocity. The summation of the polarization from the front and back crossing points of a line of sight with such a shell results in the observed EVPA of each shell either being parallel or perpendicular to the jet axis. Consequently, the integrated polarization from a cylindrical axisymmetric jet is either parallel or perpendicular to the jet axis. This is true regardless of relativistic effects and is also true in the presence of rotation of the jet (Pariev et al. 2003). Real jets are not cylindrical, and diverge with distance from the core, and they may have an elliptical or otherwise non-axisymmetric cross section. We qualitatively expect that these effects will lead to deviations of the EVPA from a strictly bimodal distribution, and even to the appearance of $\pi/4$ EVPAs with respect to the jet axis.

Polarization along or orthogonal to the jet is often interpreted in terms of toroidally or poloidally dominated jets. Since *the ratio of the toroidal to poloidal fields depends on the reference frame*, one should be careful in defining what is meant by, for example, a toroidally dominated jet. A strongly relativistic jet with comparable toroidal and poloidal fields in its rest frame (defined, for example, as a frame in which the particle distribution is isotropic) will be strongly toroidally dominated in the observer frame.

The choice of reference frame in which the structure of the jet is considered depends on the questions to be asked. For example, the intrinsic stability of the jet (e.g. with respect to kink modes) depends mostly on the properties of the jet in its rest frame. It is conjectured that strongly toroidally dominated jets (in their rest frame) should become unstable (see works on non-relativistic MHD stability of jets (Torricelli-Ciamponi & Pietrini 1990; Appl & Camenzind 1992; Appl, Lery & Baty 2000). Though there are stable laboratory field configurations with dominant toroidal fields (reverse-field pinches), they require a careful arrangement of currents that is not likely to occur under astrophysical conditions. In addition, relativistic force-free, differentially rotating pinches[1] are likely to be more stable than the non-relativistic analogue owing to the stabilizing effects of differential rotation (Istomin & Pariev 1994, 1996). However, we stress that because of the specific choice of the uniform axial magnetic field used in these works, the differential rotation might not have a stabilizing effect for more general equilibrium magnetic field configurations (see further considerations in Lyubarskii 1999; Tomimatsu, Matsuoka & Takahashi 2001). These two arguments show that the field configuration in the rest frame may be somewhat dominated by the toroidal field, but is unlikely to be strongly toroidally dominated. The observational appearance of jets, such as their intensity and linear polarization, also depends mostly on the internal structure of the jet and the emissivity distribution, but a proper transformation to the observer frame is needed. On the other hand, interactions of a jet with the surrounding medium and the corresponding instabilities (e.g. Kelvin–Helmholtz) depend on the jet properties in the observer frame (Blandford & Pringle 1976; Turland & Scheuer 1976; Hardee 1979; Bodo, Mignone & Rosner 2004).

Our polarization calculations indicate that, in the jet rest frame, the toroidal and poloidal fields are generally comparable, so that *in the observer frame, the relativistic jets are dominated by the toroidal magnetic field*: the higher the Doppler factor of the jet, the larger the observed toroidal magnetic field. Note that, in this specific case, the observed polarization electric vectors averaged over the jet size would be aligned with the jet direction, and the conclusion that the corresponding magnetic field in the jet frame is at least slightly dominated by the 'transverse' (toroidal) B-field component would, in fact, be correct. This illustrates the fact that certain of the general conclusions that have been drawn in earlier work based on observations with relatively little resolution across the jets may well be correct, even though it is true that the observed electric vectors are not, in general, orthogonal to the magnetic field. Note also that the conclusion in italics above is also consistent with the dynamical evolution of the large-scale poloidal and toroidal fields: it is expected that the ratio of the poloidal to the toroidal magnetic field in the observer frame decreases linearly with the cylindrical radius of the jet as it expands from the central disc (sizes of the order of hundreds of au) to a thickness of $\sim$0.1 pc; (see Section 7).

We also assume that the emission is optically thin and neglect possible plasma propagation effects, such as Faraday and Cotton–Mouton effects. This approximation is usually well justified (Pariev et al. 2003). Faraday rotation is absent in a pair plasma, as well as intrinsic depolarization inside the jet. VLBI polarization measurements are done at frequencies in the range 1.6 to 43 GHz. Synchrotron self-absorption is very small at GHz and higher frequencies. For $B \sim 10^{-2}$ G, $n \sim 0.1$ cm^{-3}, and $p \approx 2.5$, an approximate estimate for the synchrotron self-absorption coefficient is $\kappa_s = (5 \times 10^3 \text{ pc})^{-1}(\nu/1 \text{ GHz})^{-2-p/2}$ (e.g. Zhelezniakov 1996). The corresponding optical depth through the 1-pc jet is only 2×10^{-4}. The typical energy of particles emitting in this frequency range in a 10^{-2} G magnetic field is 100 MeV to 1 GeV. The conversion of linear polarized into circular polarized radio waves (the Cotton–Mouton effect) is also small. For both thermal and relativistic power-law particle distributions with $p \approx 2.5$ and a minimum Lorentz factor $\sim$10, the estimate for the conversion coefficient is $\kappa_c = (500 \text{ pc})^{-1}(\nu/1 \text{ GHz})^{-3}$ (Sazonov 1969). This is too small to influence the transfer of linear polarization inside the jet, but could be the source for a small circular polarization, at the level of a fraction of a per cent. We focus on linear polarization in this work.

As a first step, we consider the synchrotron emission of an unresolved, thin, circular cylindrical shell populated by relativistic electrons with a power-law distribution and moving uniformly with constant velocity $\beta = v/c$. The properties of the synchrotron emission are then determined by *three parameters*: the internal pitch angle of the magnetic field ψ', the Lorenz factor of the shell in the laboratory frame Γ and the viewing angle θ that the line of sight to the observer makes with the jet axis in the observer's reference frame. Note that, in the case of unresolved jets, this is equivalent to calculating the polarization from a jet with a pitch angle properly averaged by the emissivity.

By performing the correct Lorentz transformations of the jet and radiation electromagnetic fields, we construct polarization maps for various observation angles θ and jet parameters. We find that, in order to produce polarization along the jet axis, the pitch angle of the helical

[1] Here, by a relativistic force-free pinch, we mean that the electric fields are of the order of the magnetic fields, and the charge densities are of the order of j/nec, see below.

magnetic field *in the jet frame* must be of the order of unity or greater, $B'_\phi/B'_z \sim 1$. By virtue of the Lorentz transformation, this implies that the relativistic jets are observed to be dominated by the toroidal magnetic field $B_\phi/B_z \geqslant \Gamma$. In addition, we find that a change of the EVPA in the jet can occur only for a narrow range of rest-frame pitch angles, $\pi/4 \leqslant \psi' \leqslant \pi/3$, which allows one to measure (and not only derive a lower limit for) the ratio of the toroidal and poloidal magnetic fields: $B_\phi/B_z \sim \Gamma \gg 1$.

Further, we consider the emission from 'filled' jets, i.e. when most of the jet volume contributes to the emissivity. To find the emission properties of such jets, one also needs to integrate the jet emissivity over the jet volume. This requires knowledge of the internal structure of the jet and the distribution of synchrotron emissivity throughout the jet, which introduces large uncertainties into the model. To test the sensitivity of the results to a particular jet model, we investigate three possible force-free models for the jet structure (diffuse pinch, pinch with zero total poloidal magnetic flux and high-order reverse-field pinch) and two prescriptions for the number density of relativistic particles (proportional to the second power of the current density and to the magnetic energy density). We conclude that the emission-weighted average pitch angle in the jet must not be too small if we wish to produce longitudinal polarization. This implies that a quasi-homogeneous emissivity distribution *cannot reproduce the variety of position angle behaviour observed* – the average polarization remains primarily orthogonal to the jet, dominated by the central parts of the jet where the magnetic field in the comoving frame is primarily poloidal (since the toroidal field must vanish on the axis). Since this is not generally the case, the synchrotron emission in such jets must be generated in a narrow range of radii, where the toroidal and poloidal magnetic fields are of the same order of magnitude in the jet frame. Though Laing (1981) argued against this possibility on the grounds that it should produce strongly 'edge-brightened' profiles in resolved jets, subsequent observations of the resolved jets of Cen A (Clarke, Burns & Feigelson 1986) and M87 (Biretta, Owen & Hardee 1983) did, in fact, show such an intensity distribution.

2 SYNCHROTRON EMISSION FROM STEADY RELATIVISTIC FLOWS

Consider a cylindrical jet (Fig. 3) viewed by an observer. Below we denote all quantities measured in the local frame comoving with an elementary emitting volume with primes, while unprimed quantities are those measured in the observer's frame. Let r, ϕ and z be cylindrical coordinates centred on the jet axis and x, y and z be the corresponding rectangular coordinates. The magnetic field is in the ϕ–z direction. The components of all vectors written below are components with respect to the rectangular coordinates x, y and z. The velocity $\beta = v/c$ of the bulk motion is directed along the z-direction (the corresponding Lorentz factor is $\Gamma = 1/\sqrt{1-\beta^2}$). We do not consider bulk rotation of the jet in this work. An observer is located in the x–z plane, so that the unit vector along the direction of the emitted photons can be written $\hat{\boldsymbol{n}} = \{\sin\theta, 0, \cos\theta\}$. We denote the magnetic field in the jet by $\boldsymbol{B}$, the magnetic field in the electromagnetic wave emitted by a small volume of the jet by $\boldsymbol{b}$, the electric field in the jet by $\boldsymbol{E}$, and the electric field in the electromagnetic wave emitted by a small volume of the jet by $\boldsymbol{e}$. A hat over a vector will mean a unit vector in that direction, e.g. $\hat{\boldsymbol{B}}$ is a unit vector in the direction of the magnetic field in the observer's frame, $\hat{\boldsymbol{e}}$ is a unit vector in the direction of the electric field in the electromagnetic field in the observer's frame, $\hat{\boldsymbol{b}}'$ is a unit vector in the direction of the magnetic field in the electromagnetic wave in the comoving frame, and so on. We assume that the distribution function for the emitting particles in the frame comoving with an element of the jet is isotropic in momentum and is a power law in energy:

$$\mathrm{d}n = K_\mathrm{e}\epsilon^{-p}\,\mathrm{d}\epsilon\,\mathrm{d}V\,\mathrm{d}\Omega_{\boldsymbol{p}}. \tag{1}$$

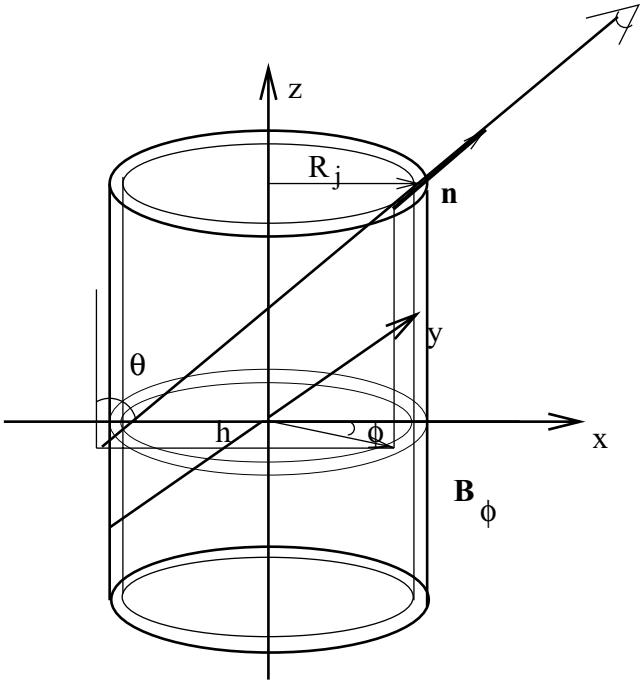

Figure 3. Geometry of the model.

Here, dn is the number of particles in the energy interval ϵ, $\epsilon + d\epsilon$, dV is the elementary volume, d$\Omega_{\boldsymbol{p}}$ is the elementary solid angle in the direction of the particle momentum $\boldsymbol{p}$, $K_{\rm e} = K_{\rm e}(r)$ and $p =$ constant.

Since the emitting particles are ultra-relativistic and we neglect the generation of circular polarization, we do not include circular polarization in our model (Stokes $V = 0$). We also neglect a possible tangled component of the magnetic field in the emission region. Under these assumptions, our estimates provide an upper limit on the possible polarization.

The Stokes parameters per unit jet length for a stationary flow are then given by (see also Lyutikov et al. 2003; Pariev et al. 2003)

$$\left.\begin{aligned} I &= \frac{p+7/3}{p+1}\frac{\kappa(\nu)}{D^2(1+z)^{2+(p-1)/2}}\int\frac{{\rm d}S}{\sin\theta}\,K_{\rm e}\,\mathcal{D}^{2+(p-1)/2}|B'\sin\chi'|^{(p+1)/2},\\ Q &= \frac{\kappa(\nu)}{D^2(1+z)^{2+(p-1)/2}}\int\frac{{\rm d}S}{\sin\theta}\,K_{\rm e}\,\mathcal{D}^{2+(p-1)/2}|B'\sin\chi'|^{(p+1)/2}\cos 2\tilde{\chi},\\ U &= \frac{\kappa(\nu)}{D^2(1+z)^{2+(p-1)/2}}\int\frac{{\rm d}S}{\sin\theta}\,K_{\rm e}\,\mathcal{D}^{2+(p-1)/2}|B'\sin\chi'|^{(p+1)/2}\sin 2\tilde{\chi},\\ V &= 0. \end{aligned}\right\} \tag{2}$$

The function $\kappa(\nu)$ is

$$\kappa(\nu) = \frac{\sqrt{3}}{4}\Gamma_{\rm E}\left(\frac{3p-1}{12}\right)\Gamma_{\rm E}\left(\frac{3p+7}{12}\right)\frac{e^3}{m_{\rm e}c^2}\left(\frac{3e}{2\pi m_{\rm e}^3c^5}\right)^{(p-1)/2}\nu^{-(p-1)/2}, \tag{3}$$

where e and $m_{\rm e}$ are the charge and mass of an electron, c is the speed of light, $\Gamma_{\rm E}$ is the Euler gamma-function, z is the cosmological redshift and D is the luminosity distance to the jet. The integration in equations (2) is over ${\rm d}S = r\,{\rm d}r\,{\rm d}\phi$, $0 < \phi < 2\,\pi$, $0 < r < R_{\rm j}$ for unresolved jets ($R_{\rm j}$ is the jet radius), while, for resolved jets ${\rm d}S = h\,{\rm d}h\,{\rm d}\phi/\sin^2\phi$, $\arcsin h/R < \phi < \pi\,{\rm sgn}\,h - \arcsin h/R$, where h is the projected distance of the line of sight from the jet axis (Pariev et al. 2003). In equation (2), $\mathcal{D}$ is the Doppler boosting factor

$$\mathcal{D} = \frac{1}{\Gamma(1-\beta\cos\theta)}, \tag{4}$$

χ' is the angle between the line of sight and the magnetic field in the rest frame of a plasma element, and $\tilde{\chi}$ is the observed EVPA in the plane of the sky seen by the observer, measured clockwise from some reference direction.

We next introduce a unit vector $\hat{\boldsymbol{l}}$ normal to the plane containing $\hat{\boldsymbol{n}}$ and the reference direction in the plane of the sky. We choose the direction of the projection of the jet axis to the plane of the sky as a reference direction, so that $\hat{\boldsymbol{l}} = \{0, 1, 0\}$. Then,

$$\cos\tilde{\chi} = \hat{\boldsymbol{e}}\times(\hat{\boldsymbol{n}}\times\hat{\boldsymbol{l}}), \quad \sin\tilde{\chi} = \hat{\boldsymbol{e}}\times\hat{\boldsymbol{l}}, \tag{5}$$

where $\hat{\boldsymbol{e}}$ is a unit vector in the direction of the electric field of the wave.

Calculation of the Stokes parameters using equations (2) is not as straightforward as in the case of a plasma at rest. Several key ingredients need to be taken into account in the case of relativistically moving synchrotron sources (Cocke & Holm 1972; Blandford & Königl 1979; Bjornsson 1982; Ginzburg 1989). First, the synchrotron emissivity depends on the angle between the direction of an emitted photon and the magnetic field in the plasma rest frame. Secondly, since emission is boosted by the bulk relativistic motion, the position angle of the linear polarization rotates parallel to the $\hat{\boldsymbol{n}}$–$\boldsymbol{v}$ plane. The fractional polarization emitted by each element remains the same, but the directions of the polarization vector of the radiation emitted by different elements are rotated by different amounts. This leads to the effective depolarization of the total emission. The theoretical maximum fractional polarization for a homogeneous field can be achieved only for a uniform plane-parallel velocity field. Thirdly, integration along the line of sight and over the image of the jet in the plane of the sky for unresolved jets is best carried out in the laboratory frame (the frame where the source is at rest as a whole).

Let $\hat{\boldsymbol{n}}'$ be a unit vector in the direction of the wave vector in the plasma rest frame, and $\hat{\boldsymbol{B}}'$ be a unit vector along the magnetic field in the plasma rest frame. The electric field of a linearly polarized electromagnetic wave $\boldsymbol{e}'$ is directed along the unit vector $\hat{\boldsymbol{e}}' = \hat{\boldsymbol{n}}'\times\hat{\boldsymbol{B}}'$ and the magnetic field of the wave $\boldsymbol{b}'$ is directed along the unit vector $\hat{\boldsymbol{b}}' = \hat{\boldsymbol{n}}'\times\hat{\boldsymbol{e}}'$. Making the Lorentz boost to the observer frame, we find (Lyutikov et al. 2003)

$$\left.\begin{aligned} \hat{\boldsymbol{n}}' &= \frac{\hat{\boldsymbol{n}}+\Gamma\boldsymbol{v}\left[\frac{\Gamma}{\Gamma+1}(\hat{\boldsymbol{n}}\times\boldsymbol{v})-1\right]}{\Gamma\left[1-(\hat{\boldsymbol{n}}\times\boldsymbol{v})\right]},\\ \hat{\boldsymbol{e}} &= \frac{\hat{\boldsymbol{n}}\times\boldsymbol{q}'}{\sqrt{q'^2-(\hat{\boldsymbol{n}}\times\boldsymbol{q}')^2}},\\ \boldsymbol{q}' &= \hat{\boldsymbol{B}}'+\hat{\boldsymbol{n}}\times(\boldsymbol{v}\times\hat{\boldsymbol{B}}')-\frac{\Gamma}{1+\Gamma}(\hat{\boldsymbol{B}}'\times\boldsymbol{v})\boldsymbol{v}, \end{aligned}\right\} \tag{6}$$

where here and in all further expressions we set $c = 1$. We can express the rest-frame unit vector $\hat{\boldsymbol{B}}'$ in terms of the unit vector $\hat{\boldsymbol{B}}$ along the magnetic field in the laboratory frame. Assuming ideal MHD, there is no electric field in the plasma rest frame, $\boldsymbol{E}' = 0$. We then obtain

$$\left.\begin{aligned} \hat{\boldsymbol{B}} &= \frac{1}{\sqrt{1-(\hat{\boldsymbol{B}}'\times\boldsymbol{v})^2}}\left[\hat{\boldsymbol{B}}'-\frac{\Gamma}{1+\Gamma}(\hat{\boldsymbol{B}}'\times\boldsymbol{v})\boldsymbol{v}\right],\\ \hat{\boldsymbol{B}}' &= \frac{(1+\Gamma)\hat{\boldsymbol{B}}+\Gamma^2(\hat{\boldsymbol{B}}\times\boldsymbol{v})\boldsymbol{v}}{(1+\Gamma)\sqrt{1+\Gamma^2(\hat{\boldsymbol{B}}\times\boldsymbol{v})^2}}, \end{aligned}\right\} \tag{7}$$

to get

$$\left.\begin{aligned}\hat{\boldsymbol{e}} &= \frac{\hat{\boldsymbol{n}}\times\boldsymbol{q}}{\sqrt{q^2-(\hat{\boldsymbol{n}}\times\boldsymbol{q})^2}},\\ \boldsymbol{q} &= \hat{\boldsymbol{B}}+\hat{\boldsymbol{n}}\times(\boldsymbol{v}\times\hat{\boldsymbol{B}}).\end{aligned}\right\} \tag{8}$$

This is a general expression giving the polarization vector in terms of the observed quantities $\hat{\boldsymbol{B}}$, $\hat{\boldsymbol{n}}$ and $\boldsymbol{v}$. Quite compact form of expression (8) was derived in (Lyutikov et al. 2003).

Relativistic aberration makes the observed electric field in the wave non-orthogonal to the observed B field and to its projection on the sky. Owing to the conservation of the relativistic invariant $\boldsymbol{e}'\times(\boldsymbol{b}'+\boldsymbol{B}')$, we find that (see also Blandford & Königl 1979)

$$\boldsymbol{e}\times\boldsymbol{B}=(\boldsymbol{v}\times\boldsymbol{B})\times(\hat{\boldsymbol{n}}\times\boldsymbol{e}). \tag{9}$$

For example, the angle between $\hat{\boldsymbol{e}}$ (which lies in the plane of the sky) and $\hat{\boldsymbol{B}}$ is

$$\cos\zeta=\hat{\boldsymbol{e}}\times\hat{\boldsymbol{B}}=\frac{(\hat{\boldsymbol{B}}\times\hat{\boldsymbol{n}})\left[\hat{\boldsymbol{B}}\times(\hat{\boldsymbol{n}}\times\boldsymbol{v})\right]}{\sqrt{q^2-(\hat{\boldsymbol{n}}\times\boldsymbol{q})^2}}, \tag{10}$$

which is in general not equal to zero. The observed electric field is orthogonal to the observed B field if either $\hat{\boldsymbol{B}}$ lies in the $\hat{\boldsymbol{n}}$–$\boldsymbol{v}$ plane or $(\hat{\boldsymbol{B}}\times\hat{\boldsymbol{n}})=\boldsymbol{0}$.

Next, we apply the above general relations to the case of synchrotron emission by a thin cylindrical shell carrying toroidal magnetic field and moving uniformly with velocity β parallel to its axis in the z-direction. The shell is viewed at an angle θ with respect to its axis, so that

$$\left.\begin{aligned}\boldsymbol{v} &= \beta\{0,0,1\}\\ \hat{\boldsymbol{n}} &= \{\sin\theta,0,\cos\theta\}.\end{aligned}\right\} \tag{11}$$

Let the magnetic field $\boldsymbol{B}'$ in the emitting shell in the jet frame be helical:

$$\left.\begin{aligned}\boldsymbol{B}' &= B'_{\phi}\{-\sin\phi,\cos\phi,0\}+B'_{z}\{0,0,1\}=B'\sin\psi'\{-\sin\phi,\cos\phi,0\}+B'\cos\psi'\{0,0,1\}\\ \boldsymbol{B}' &= B'\hat{\boldsymbol{B}}',\quad \hat{\boldsymbol{B}}'=\sin\psi'\{-\sin\phi,\cos\phi,0\}+\cos\psi'\{0,0,1\},\end{aligned}\right\} \tag{12}$$

where ψ' is the magnetic field pitch angle in the shell rest frame, $\hat{\boldsymbol{B}}'$ is a unit vector along the magnetic field in the shell frame, and B' is the magnitude of the field. At this point, we are interested in the emission of a single shell and do not specify, for the moment, the radial dependence of the magnetic fields and emissivities. This is considered in Section 4.

For this particular choice of geometry, we find

$$\hat{\boldsymbol{n}}'=\mathcal{D}\left[\sin\theta,0,\Gamma(\cos\theta-\beta)\right], \tag{13}$$

$$\hat{\boldsymbol{B}}=\frac{1}{\sqrt{1-\beta^2\cos^2\psi'}}\left(-\sin\psi'\sin\phi,\cos\phi\sin\psi',\frac{\cos\psi'}{\Gamma}\right), \tag{14}$$

$$\cos\chi'=(\hat{\boldsymbol{n}}'\times\hat{\boldsymbol{B}}')=\mathcal{D}\left[\Gamma\cos\psi'(\cos\theta-\beta)-\sin\theta\sin\phi\sin\psi'\right], \tag{15}$$

where $\hat{\boldsymbol{B}}$ is the unit vector along the magnetic field in the laboratory (observer) frame. Note that

$$\left.\begin{aligned}\hat{\boldsymbol{B}}\times\hat{\boldsymbol{n}} &= \frac{\cos\theta\cos\psi'-\Gamma\sin\theta\sin\phi\sin\psi'}{\Gamma\sqrt{1-\beta^2\cos^2\psi'}},\\ \hat{\boldsymbol{B}}\times\boldsymbol{v} &= \frac{\beta\cos\psi'}{\Gamma\sqrt{1-\beta^2\cos^2\psi'}},\\ \hat{\boldsymbol{B}}\times\hat{\boldsymbol{n}}\times\boldsymbol{v} &= -\frac{\beta\sin\theta\sin\psi'\cos\phi}{\sqrt{1-\beta^2\cos^2\psi'}}.\end{aligned}\right\} \tag{16}$$

The pitch angle in the laboratory frame, ψ, is larger than in the rest frame:

$$\tan\psi=\Gamma\tan\psi'. \tag{17}$$

As we have already pointed out, one of the main effects of the relativistic Lorentz transformation is that the observed magnetic field and polarization vectors are not, in general, orthogonal (Blandford & Königl 1979). For cylindrical jets, the expression for the angle ζ is too lengthy to be reproduced here (see also Appendix A). The dependence of ζ on ϕ is plotted in Fig. 4. In Fig. 5, we plot the observed relative orientations of the electric field in the wave and the magnetic field projected on to the plane of the sky. Note that, for a stationary jet, the electric field is always perpendicular to the magnetic field, while this is no longer true for a relativistically moving jet. In fact, *the electric field of the wave may become almost parallel to the magnetic field for some viewing angles*.

The degree of linear polarization of the observed radiation is $\Pi=\sqrt{Q^2+U^2}/I$. The resultant EVPA measured by the observer, $\tilde{\chi}_{\rm res}$, is obtained from

$$\cos 2\tilde{\chi}_{\rm res}=\frac{Q}{\sqrt{Q^2+U^2}},\quad \sin 2\tilde{\chi}_{\rm res}=\frac{U}{\sqrt{Q^2+U^2}},\quad 0\leqslant\tilde{\chi}_{\rm res}<\pi. \tag{18}$$

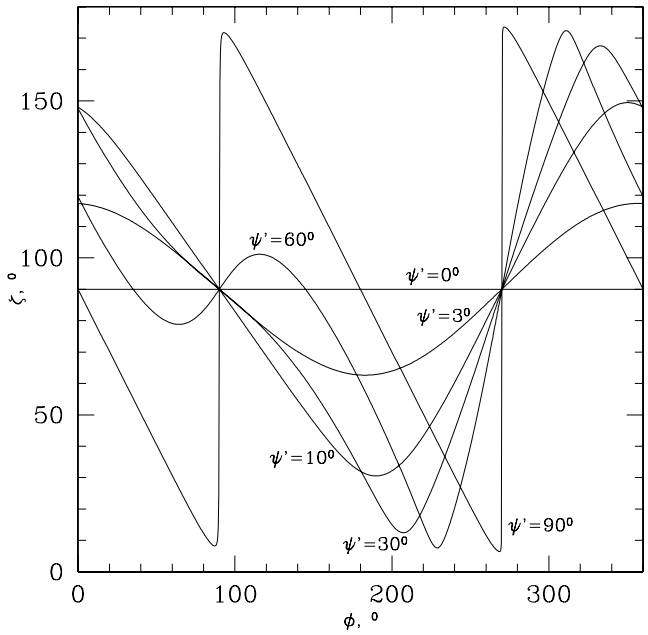

Figure 4. Angle ζ between the observed direction of the magnetic field $\hat{\boldsymbol{B}}$ and the polarization vector in the wave as a function of ϕ for a cylindrical shell with $\Gamma = 10$, $\theta = 0.1$ and six values of ψ'. In accordance with formula (10), $\zeta = 90^\circ$ when either the magnetic field is purely axial ($\psi' = 0$) or at the visible edges of the jet ($\phi = 90^\circ$ and $\phi = 270^\circ$).

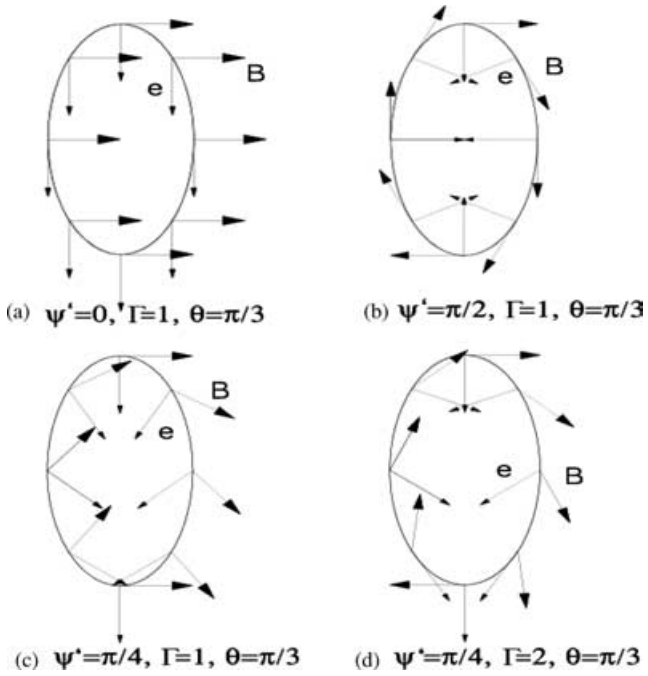

Figure 5. Examples of observed electric field in the wave and magnetic field for $\theta = \pi/3$. Projections of the magnetic field on the plane of the sky are denoted by arrows with large head, electric fields are denoted by arrows with small heads. (a) Purely poloidal magnetic field $\psi' = 0$, (b) toroidal magnetic field $\psi' = \pi/2$, (c) helical field with $\psi' = \pi/4$ viewed in the rest frame, (d) helical field with $\psi' = \pi/4$ moving with $\Gamma = 2$. For stationary jets (a–c) the electric vector of the wave is always orthogonal to the magnetic field in the jet in the observer frame; for moving jets (case d) this is not true anymore.

It can be verified that, for a cylindrically symmetric flow and magnetic field, the change of ϕ to $\pi - \phi$ in the integrals (2) does not change the value of Q and the sign of U is reversed. Therefore, the Stokes parameter U integrates to zero. Consequently, if $Q > 0$ then $\tilde{\chi}_{\rm res} = 0$, and if $Q < 0$ then $\tilde{\chi}_{\rm res} = \pi/2$. Thus, *for circular jets, the observed EVPA can be either parallel or perpendicular to the projection of the jet axis on to the plane of the sky*. This is true for differentially rotating jets as well (Pariev et al. 2003). This naturally explains the observed bimodal distribution of the jet EVPAs.

Since $U = 0$ for a circular jet, we define the fractional polarization as $\Pi = Q/I$, retaining the sign of Q, so that Π can be smaller than zero. For $\Pi > 0$, the polarization is along the jet, while the polarization is orthogonal to the jet for $\Pi < 0$.

Given that the angle between the observed EVPA and observed magnetic field for individual radiating plasma elements are not, in general, orthogonal, depending on the viewing conditions, we can ask why it is the case that reasonably clear patterns have appeared in the relationship between the observed EVPAs and the local jet direction. This can be understood, in part, as a consequence of the fact that the resolution provided by VLBI observations is often insufficient fully to resolve the jets in the transverse direction, so that the EVPA integrated over the jet cross section is observed. This is essentially equivalent to the statement above that the observed EVPA *integrated over a cylindrical jet* is expected to be either parallel or perpendicular to the projection of the jet axis on to the plane of the sky. The observed EVPA will essentially be determined by the ratio B'_ϕ/B'_z; if the jets are approximately cylindrical, the observed EVPA can be used to draw conclusions about the ratio of the toroidal and poloidal magnetic field components in the rest frame, but it is not always possible to translate these into unambiguous conclusions about this ratio in the observer's frame. (Note, however, that most conclusions about the *B*-field direction that have been inferred from the direction of the EVPA have, in fact, implicitly taken this to mean the *B*-field in the source rest frame.)

3 HOLLOW CYLINDRICAL JETS

3.1 Unresolved hollow jets (cylindrical shell)

We first consider cylindrical jets with their emissivity confined to a narrow cylindrical shell. In order to interpret observations that do not resolve the transverse dependence of the polarization across the jet, we integrate the emissivity of the shell over the azimuthal angle in the observer's frame. For a constant velocity field of the shell, all relativistic effects can be accounted for by the Lorentz transformation: the degree of polarization can be calculated in the jet rest frame for the viewing angle in the jet rest frame θ' obtained from expression (13)

$$\sin\theta' = \frac{\sin\theta}{\Gamma\,(1-\beta\cos\theta)}, \quad \cos\theta' = \frac{\cos\theta-\beta}{1-\beta\cos\theta}, \tag{19}$$

where $0 < \theta < \pi$ and $0 < \theta' < \pi$. In addition, the Lorentz transformation of the jet magnetic field is $B_z = B'_z$, $B_\phi = \Gamma\ B'_\phi$ and results in the change of the pitch angle described by expression (17). Though corresponding non-relativistic calculations have been done by Laing (1981), the interpretation of these calculations for a relativistically moving shell is different.

The general expressions for polarization given in Section 2 can be simplified considerably for non-relativistic jets. Setting $\beta = 0$, we find

$$\left.\begin{aligned} \sin^2\chi' &= \cos^2\psi'\sin^2\theta + \frac{1}{2}\sin 2\theta\sin 2\psi'\sin\phi + (\cos^2\theta+\cos^2\phi\sin^2\theta)\sin^2\psi' \\ \cos 2\tilde{\chi} &= \frac{\cos^2\phi\sin^2\psi' - (\cos\psi'\sin\theta+\cos\theta\sin\phi\sin\psi')^2}{1-(\cos\theta\cos\psi'-\sin\theta\sin\phi\sin\psi')^2}. \end{aligned}\right\} \tag{20}$$

The degree of polarization Π from a cylindrical shell populated by particles with various power-law indices $p = 1, 2.4, 3$ are plotted in Fig. 6 as a function of the viewing angle and pitch angle (see also Laing 1981). (A typical power-law index for pc-scale jets is $p = 2.4$, which corresponds to a spectral index of $\alpha = -0.7$, $S_\nu \propto \nu^\alpha$; see, for example, Gabuzda & Gómez 2001; Gabuzda, Gómez & Aguda 2001b.)[2] As can be seen from Fig. 6 (positive values indicate polarization along the jet, and negative values polarization orthogonal to the jet), there is a weak dependence of the polarization on the spectral index. In particular, flatter spectra (smaller p) produce more complicated polarization structure, so that *sources with flatter spectra are more likely to produce a change of polarization from parallel to perpendicular*.

For relativistic jets, we adopt $p = 2.4$ as a fiducial number and plot the fractional polarization for various viewing angles and pitch angles in the rest frame and the laboratory frame (Fig. 7). In addition, we plot in Fig. 8 the fractional polarization as a function of the bulk Lorentz factor Γ for $\theta = 10^\circ$.

Several conclusions can be drawn upon analysing these plots. Consider first the polarization as a function of the viewing angle for various rest-frame pitch angles (Fig. 7a). For extreme values of the pitch angle in the rest frame (purely toroidal magnetic field, $\psi' = \pi/2$, and purely poloidal magnetic field $\psi' = 0$), the corresponding polarization is along ($\Pi > 0$) and orthogonal ($\Pi < 0$) to the jet. For large pitch angles, $\pi/3 \leqslant \psi' \leqslant \pi/2$, the polarization always remains along the axis, peaking at $\theta \sim 1/\Gamma$ and decreasing sharply for $\theta\Gamma \gg 1$. For intermediate pitch angles, $\psi' \leqslant \pi/3$, the polarization can change from parallel to orthogonal depending on the viewing angle, with such a change being more likely to occur for lower values of p. For smaller pitch angles, $\psi' \leqslant \pi/4$, the polarization is high, weakly dependent on the viewing angle, and oriented orthogonal to the jet.

Thus, the average polarization is a very sensitive function of the jet parameters. For some jet parameters, the polarization properties are fairly constant, while, in some cases, they can change appreciably due to small variations in the jet parameters.

Most importantly, the observation of polarization along the jet requires that the toroidal magnetic field *in the jet frame* be at least of the order of the poloidal field. For relativistic jets, this means that such jets are *strongly dominated by the toroidal field in the observer's frame*, $B_\phi/B_z \sim \Gamma\ B'_\phi/B'_z \gg 1$. In cases when a change of sign is seen, we can place strong constraints on the internal pitch angle, since such

[2] A particularly simple case is $p = 3$, when the integrations in equations (2) can be done exactly (see also Pariev et al. 2003, for another exactly integrable case). We find for the average polarization of an unresolved shell:
$$\Pi = -(3/2)(1+3\cos 2\psi')\sin^2\theta(5-\cos 2\theta-\cos 2\psi'-3\cos 2\theta\cos 2\psi')^{-1} \tag{21}$$

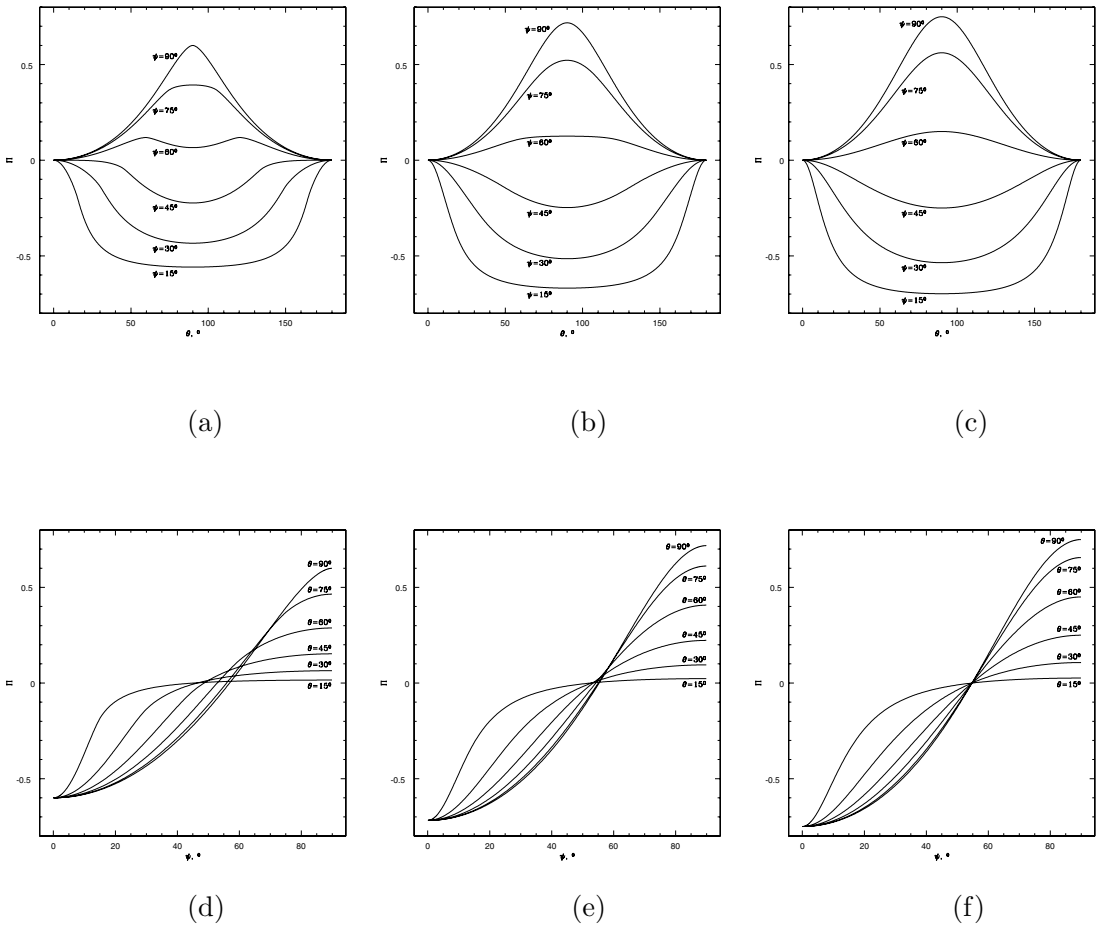

Figure 6. Polarization fraction $\Pi = Q/I$ for non-relativistic cylindrical shells. First row of plots are Π as a function of the observer angle θ for $p = 1$ (a), 2.4 (b), 3 (c); second row of plots are Π as a function of the pitch angle ψ' for $p = 1$ (d), 2.4 (e), 3 (f). Positive values indicate polarization along the jet; negative – polarization orthogonally to the jet.

transitions can be seen only for a limited range of pitch angles, $\pi/3 \leqslant \psi' \leqslant \pi/4$. A 90° change of the EVPA can be initiated by already a small deviation of the jet direction caused, for example, by the precession of the jet base (if $\theta \sim 1/\Gamma$, in order to change the observed EVPA by an angle of the order of unity, the real direction may change by $\Delta\theta \ll 1/\Gamma$). Similarly, a slight acceleration of the jet or injection of a small amount of the additional toroidal magnetic flux (as in the 'sweeping magnetic twist' model of Nakamura, Uchida & Hirose 2001 and Kigure et al. 2004). On the other hand, a relativistic jet viewed at a large angle, $\theta \gg 1/\Gamma$, will be either weakly polarized along the jet (for $B'_\phi \geqslant B'_z$) or strongly polarized orthogonally to the jet (for $B'_\phi \leqslant B'_z$); see Fig. 7a.

3.2 Resolved hollow jets (cylindrical shells)

We next turn to resolved jets. If emission is confined to a narrow cylindrical shell, $K_{\rm e} \propto \delta(r - R_{\rm j})$ then integration over dS gives a multiplier $h/\arcsin h/R_{\rm j}$, so that polarization becomes

$$\Pi = \frac{p+1}{p+7/3}\cos 2\tilde{\chi}. \tag{22}$$

In Fig. 9 we plot the fractional polarization for shells moving with $\Gamma = 10$, for various pitch angles ψ' and viewing angles θ.

First, note that the polarization close to the edge of the observed jet is always orthogonal to the jet. This can easily be understood from simple geometrical considerations: at the visible edge of the cylindrical shell, the projection of the toroidal magnetic field on to the plane of the sky becomes zero, so that only the poloidal magnetic field contributes to the observed synchrotron emission, and this part of the jet is observed to be polarized orthogonal to the jet axis. For $\theta \ll 1/\Gamma$ and $\theta \gg 1/\Gamma$, the polarization in the central part of the jet is along the symmetry axis. Also, in both cases of very large ($\theta \gg 1/\Gamma$) and very small ($\theta \ll 1/\Gamma$) viewing angles, the profile of the polarization becomes close to symmetric with respect to the jet axis. For intermediate values of $\theta \sim 1/\Gamma$, the polarization in the central parts of the jet is longitudinal if the pitch angle $\psi' > 45°$ and orthogonal if $\psi' < 45°$. This can explain in a natural way the fact that resolved jets sometimes have polarization aligned with the jet in the central region and orthogonal to the jet at the edge.

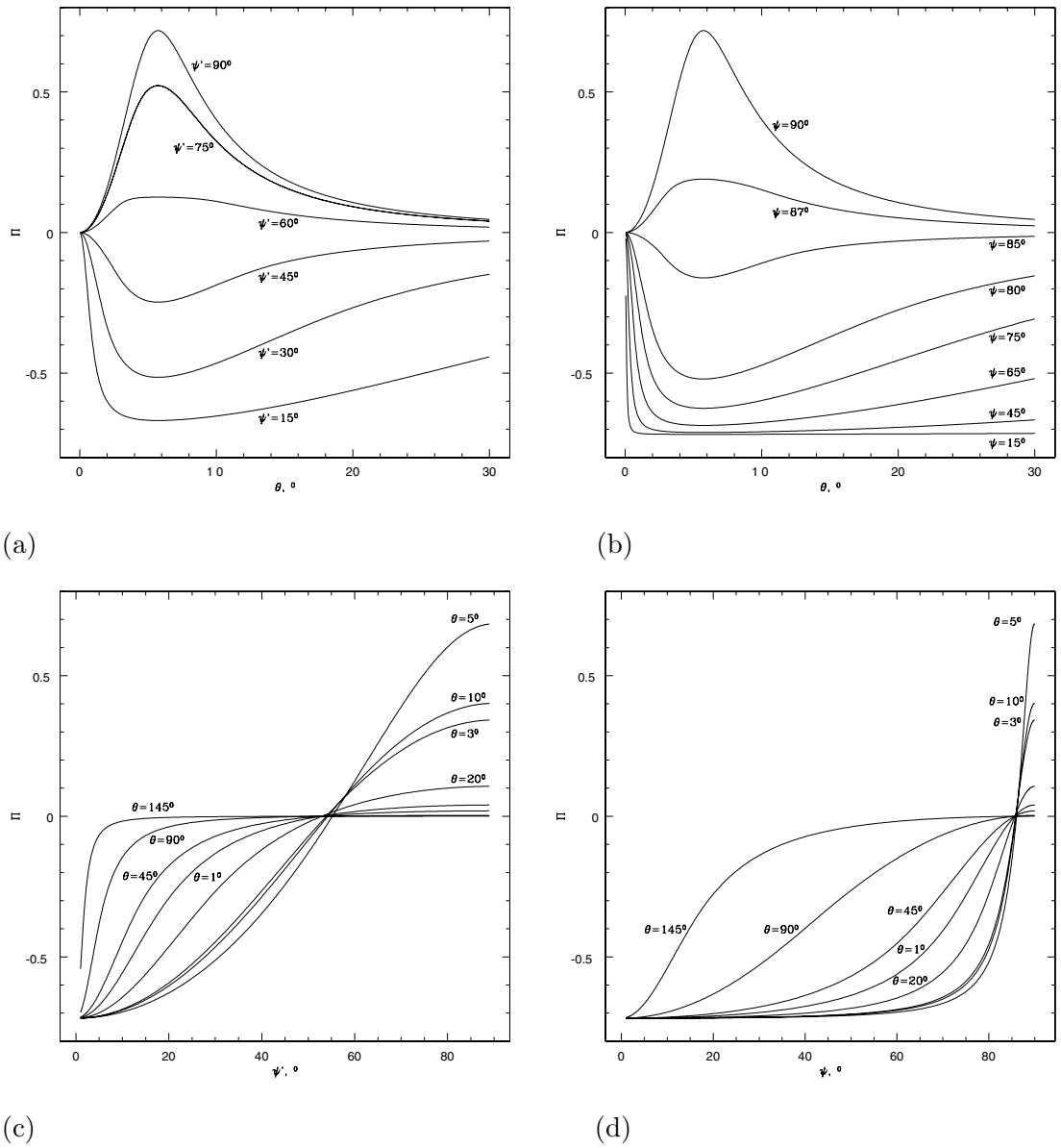

Figure 7. Polarization fraction for cylindrical shells with $\Gamma = 10$ and particle index $p = 2.4$ as a function of the observer angle θ for different values of rest-frame pitch angle ψ' (a) and for different values of laboratory frame pitch angle ψ (b); for different values of the observer angle θ as a function of the rest-frame pitch angle ψ' (c) and laboratory frame pitch angle ψ (d).

Secondly, *polarization observations of resolved jets can be used to infer the relative orientation of the spin of the central object that launched the jet (black hole or disc): whether it is aligned or counter-aligned with the jet axis.* This possibility comes from the fact that the *left- and right-handed helices produce different polarization signatures,* see Fig. 9. In order to make a distinction between the two choices, it is necessary to determine independently the angle at which the jet is viewed in its rest frame. For ultra-relativistic jets, this amounts to determining the product $\theta\Gamma$: if $\theta\Gamma < 1$ then the jet is viewed 'head-on', while the jet is viewed 'tail-on' if $\theta\Gamma > 1$. A right-handed magnetic helix viewed head-on produces the same polarization signature as a left-handed helix viewed tail-on. A left-handed magnetic helix viewed head-on produces the same polarization signature as a right-handed helix viewed tail-on. Right-handed helices correspond to the case of the same signs of B_z and B_ϕ and left-handed helices correspond to the case of the opposite signs of B_z and B_ϕ (in the standard, right-handed coordinate system r, ϕ, z as shown in Fig. 3).

We expect that the magnetic field lines in the jet are retrograde with respect to the black hole spin. Thus, if the spin of the central object is oriented parallel to the z-direction but to the negative z, counter-aligned with the direction of the jet (i.e. the black hole rotates clockwise if viewed by the observer on Fig. 3), the magnetic field lines will form a right-handed helix (see Fig. 10). Suppose next that we view the jet at angles $\theta\Gamma < 1$, so that, in the frame of the jet, a circular right-handed helix is moving toward an observer along the z-axis. A spiral magnetic field given by equations (12) forms a right-handed spiral. Let us denote by l the coordinate along the unit vector $\hat{\boldsymbol{l}} = \{0, 1, 0\}$ in the plane of the sky parallel to the y-axis. In this case, the parts of the jet located at negative l will be more preferentially polarized along the jet

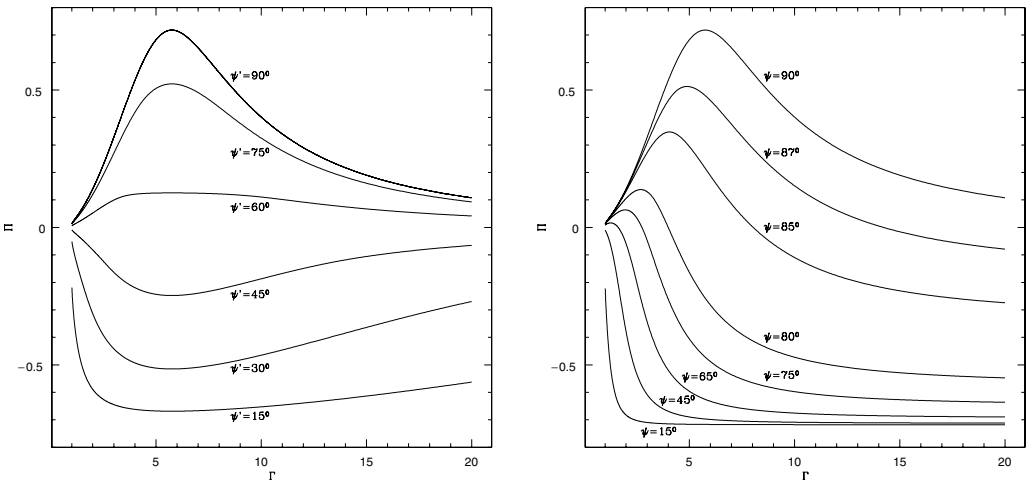

Figure 8. Polarization fraction for a cylindrical shell as a function of Lorentz factor Γ for different rest-frame and laboratory frame pitch angles ψ' and ψ. Viewing angle $\theta = 10^\circ$ and $p = 2.4$.

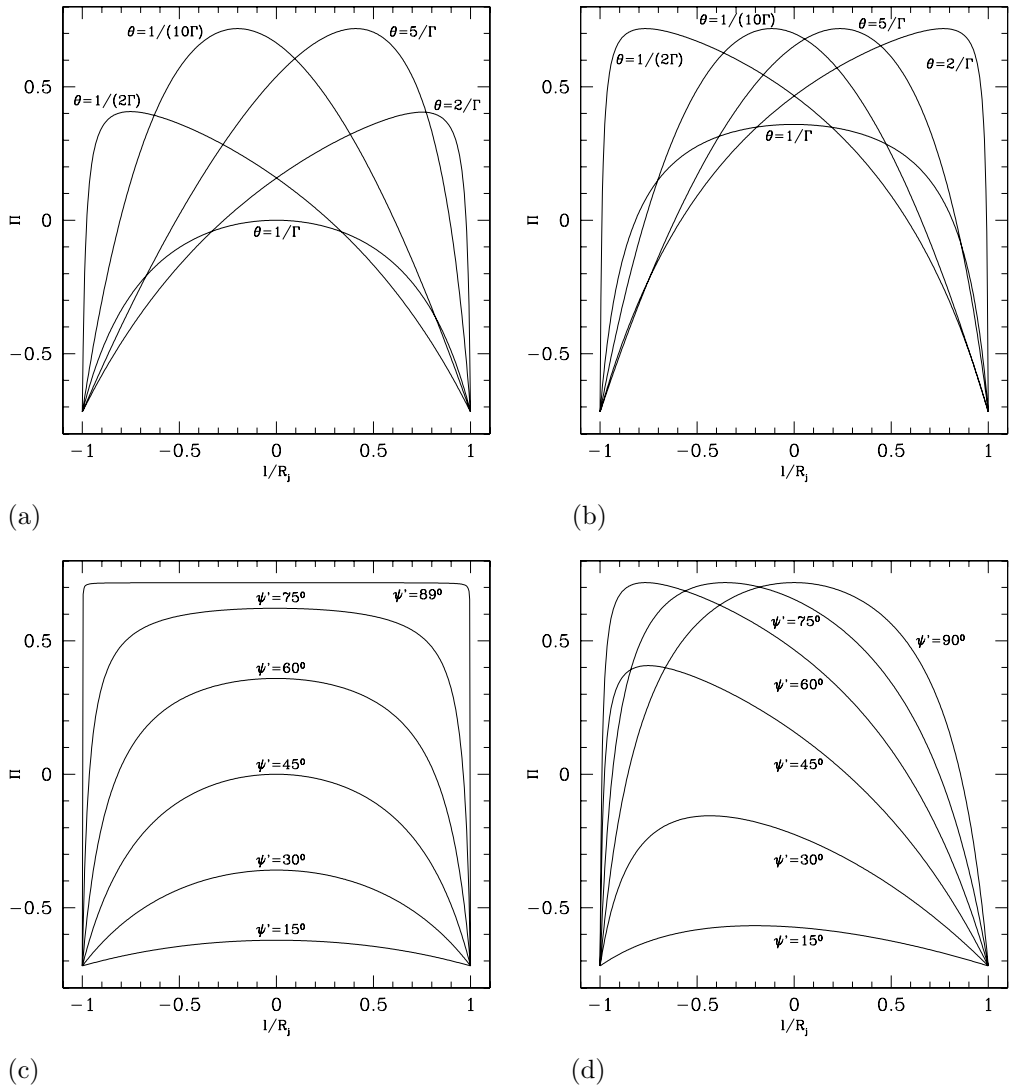

Figure 9. Profiles of the polarization degree Π for resolved cylindrical shells as a function of the distance across the jet projected on the sky, l. The radius of the shell, R_j, is arbitrary. $\Gamma = 10$ and $p = 2.4$. The plots a are for $\psi' = 45^\circ$, and plots b are for $\psi' = 60^\circ$ for the different values of the viewing angle θ. Plots c are for $\theta = 1/\Gamma$, and plots d are for $\theta = 1/(2\Gamma)$ for the different values of the pitch angle ψ'. For small and large θ, the polarization in the central part of the image is along the axis of the jet regardless of the value of ψ'. For $\theta \sim 1/\Gamma$ the polarization can be longitudinal only for $\psi' > 45^\circ$. At the edge of the jet the polarization is orthogonal to the jet axis for any values of θ and ψ'.

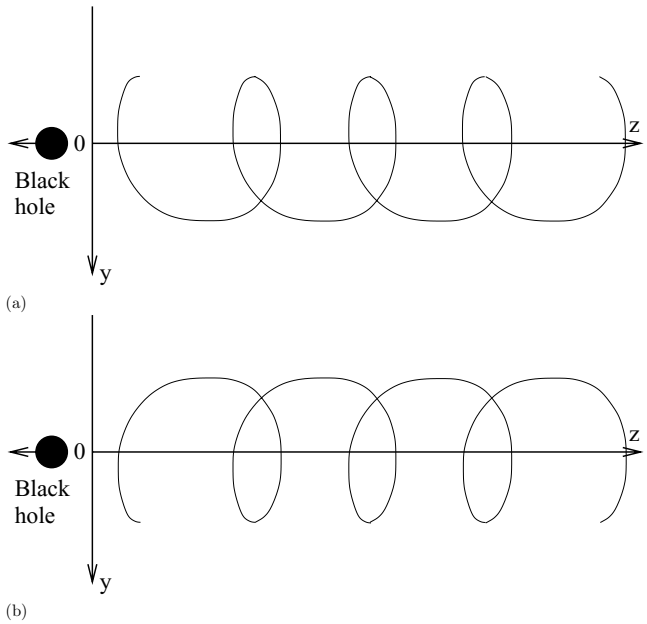

Figure 10. 'Head-on' ($\theta\Gamma < 1$) (plot a) and 'tail-on' ($\theta\Gamma > 1$) (plot b) views of a right-handed helical magnetic field in the reference frame comoving with the jet in the positive z-direction. The location of the observer is the same as in Fig. 3. For a 'head-on' viewer, polarization Π of the lower, $y > 0$, part is lower (that it more negative, in the algebraic sense) than the polarization of the upper, $y < 0$ part, i.e. it is more likely to be perpendicular to the jet. For a 'tail-on' viewer, polarization Π of the lower, $y > 0$, part is larger (that is more positive, in the algebraic sense) than the polarization of the upper, $y < 0$, part, i.e. it is more likely to be parallel to the jet. These trends in polarization correspond to the small and large angle curves plotted on Fig. 9, plots a and b.

(that is, Π will be more positive, in the algebraic sense), than the parts of the jet located at positive l. For example, for $\theta = 1/(2\Gamma)$ and $\psi' = 45^\circ$ ('head-on' right-handed helix), the value of Π is positive and the polarization is along the jet over the range in l/R_j from about -0.98 to 0.25 (see the $\theta = 1/2\Gamma$ curve in Fig. 9a). For $\theta = 5/\Gamma$ and $\psi' = 45^\circ$ ('tail-on' right-handed helix), the value of Π is positive and the polarization is along the jet over the range in l/R_j from about -0.5 to 0.9 (see the $\theta = 5/\Gamma$ curve in Fig. 9a). While for a more tightly wound spiral, $\psi' = 60^\circ$ (Fig. 9b), the range in l/R_j where $\Pi > 0$ becomes wider than for $\psi' = 45^\circ$, the asymmetry of the profile of Π versus l remains in place: for $\theta < 1/\Gamma$ the range of positive Π is shifted toward negative l and for $\theta > 1/\Gamma$ the range of positive Π is shifted toward positive l (compare this with the Π versus ψ' dependencies shown in Figs 9c and d).

The results of calculations presented in Fig. 9 are invariant with respect to simultaneous sign changes of both the B_z and B_ϕ components of the magnetic field. Such reversal of the magnetic field preserves the property of the magnetic helix to be right- or left-handed, and the polarization properties are unchanged. In the case of the spin of the central object being aligned with the direction of the jet, the black hole or accretion disc rotates clockwise when viewed by an observer looking down the jet. Polarization curves for a left-handed helix are obtained from polarization curves for a right-handed helix, Figs 9a and b, by flipping l to $-l$, i.e. a value of Π at some location l/R_j for a left-handed helix is equal to the value of Π at a location $-l/R_\mathrm{j}$ (and the same Γ, θ and ψ') for a right-handed helix. Therefore, the trends in the profiles of Π across the jet are reversed for a left-handed helix: for 'head-on' viewing the maximum in the polarization curve $\Pi(l)$ (in the algebraic sense) is shifted toward positive values of l and for 'tail-on' viewing the maximum in the polarization curve $\Pi(l)$ (in the algebraic sense) is shifted toward negative values of l.

The direction of the jet axis can be defined by the symmetry of the intensity profile, so that the direction of the black hole spin can be determined from the asymmetry of the polarization profile when measured perpendicular to this axis (see Figs 9a, b and d). The intensity profile itself will also be asymmetric, so it cannot be easily used to infer the exact location of the symmetry axis of the magnetic spiral. However, it is sufficient to know only the direction of this axis, as all polarization profiles are skewed toward one side, namely the side where Π is more positive. If an observer positions himself along the projection of the jet on to the plane of the sky (z-axis on Fig. 10) with his head toward the end point of the jet and his feet toward the core of the AGN, then the side of the jet with negative l will be on his left side, and the side of the jet with positive l will be on his right side. Then, a head-on viewed jet ($\theta < 1/\Gamma$) emanating from a clockwise rotating central engine has the maximum of Π on the left side of its image on the sky, while a head-on viewed jet emanating from a counter-clockwise rotating central engine has the maximum of Π on the right side of its image on the sky. The opposite holds for a tail-on viewed jet ($\theta > 1/\Gamma$): jets emanating from a clockwise rotating central engine have the maximum of Π on the right side of their image on the sky, while jets emanating from a counter-clockwise rotating central engine have the maximum of Π on the left side of their image on the sky. When $\theta \approx 1/\Gamma$, i.e. when the jet is viewed orthogonal to its axis in the frame comoving with the jet, the $\Pi(l)$ curve becomes symmetric with respect to the jet axis (Fig. 9c). We stress once again that the maximum of Π is considered here in the algebraic sense taking into account our agreement on the sign of Π, i.e. either we take the maximum of the absolute value of the degree of longitudinal polarization, or the minimum of the absolute value of the degree of perpendicular polarization, if the polarization is perpendicular at any location across the jet.

The caveat here is how one can know if a jet is viewed head-on or tail-on in its rest frame. Because the parsec-scale counter-jet is almost always not observed, we do not readily see how to overcome this caveat. The measurements of the intensity profile across the jet will not help to resolve this ambiguity, because the intensity profiles must obey all invariance properties that polarization profiles do (this is evident from general expressions 2). In general, it is the polarization properties that could give us additional information that can break the insensitivity of the intensity profiles to some parameters (degeneracy), and not the other way around.

4 EMISSION FROM 'FILLED' JETS

To find the total emission from a jet, we must know the distribution of the emissivity and the internal structure of the jet, both of which are highly uncertain functions. In this section we consider emission from jets with force-free magnetic field structure. There are two reasons to consider force-free jets. First, any MHD jet will evolve toward a force-free configuration (plus an helicity conservation constraint), provided that the outside conditions do not change too rapidly (e.g. Choudhuri & Konigl 1986). Secondly, it is probable that jets are electromagnetically dominated on parsec scales (Lynden-Bell 1996, 2003; Ustyugova et al. 2000; Li et al. 2001; Lovelace et al. 2002; Lovelace & Romanova 2003; see also Section 6), so that their structure is determined by relativistic force-free electrodynamics. In this work, we assume that the jets are strongly magnetized and are described by relativistic force-free electrodynamics. In Appendix B, we present equations of relativistic force-free electrodynamics and suggest a simple method that can be used to find a broad class of solutions for cylindrical, relativistic, force-free pinches given the corresponding non-relativistic pinches.

There are many ways in which the poloidal magnetic field, electric charge and poloidal current can be distributed inside a jet. This should depend primarily on the jet launching conditions (as boundary conditions) and the evolution of the jet as it propagates. At the moment, there is no general agreement about the structure of jets. Furthermore, it is not even clear if jets carry a total poloidal current and total poloidal magnetic flux. It is likely that jets do carry total current, as models for the launching and collimation of jets show (Blandford & Payne 1982; Contopoulos & Lovelace 1994; Ustyugova et al. 2000; Lovelace et al. 2002). Whether there is a total poloidal magnetic flux is less clear. Most models for jet launching assume that there is a large poloidal magnetic flux at the base of the jet, but physically it is hard to see how this large-scale field survives in a turbulent disc. An alternative possibility is that magnetorotational instability operating in the disc produces complicated field structures with negligible total poloidal flux. One advantage of these models is that the energy associated with current reversals can be used to power the jet (e.g. Lovelace, Newman & Romanova 1997).

There is a multitude of possible jet profiles, each giving a different polarization structure (also with a number of different prescriptions for the jet emissivity). Given these uncertainties, we consider below three types of jet structure: (i) a diffuse pinch with large poloidal and toroidal field fluxes; (ii) a particular example of an infinite (single) reverse-field pinch with vanishing total poloidal magnetic flux; and (iii) a high-order reverse-pinch configuration. We believe that these three sample jet structures are generic examples and somewhat at the extreme ends of expected cases in terms of their total poloidal field flux, which is logarithmically divergent for (i) and zero for (ii) and (iii). The current density is concentrated toward the centre of the jet in all cases considered, forming the core of the jet. The total energy of the magnetic field is also finite, and the spatial distribution of the magnetic-field energy is concentrated inside a core of the same typical radius as the current-carrying core of the jet. Below, we denote the radius of the jet core as $R_{\rm j}$ and its inverse as $a = 1/R_{\rm j}$.

In addition, the distribution of emissivity in the jet must also be specified. We consider here the consequences of the hypothesis that dissipation and particle acceleration occur throughout the jet volume, as opposed to the dissipation being localized in current reconnection layers (Lyutikov & Uzdensky 2003) or resonant layers of electromagnetic perturbations (Beresnyak, Istomin & Pariev 2003). Although the exact dissipation rate may depend on micro-physical and kinetic processes, it is reasonable to assume that the dissipation rate is given by the Ohmic heating in the rest frame of a plasma element, j'^2/σ', where j' is the absolute value of the current density and σ' is the conductivity in a frame comoving with the plasma element. Some fraction of this dissipated energy is then converted into heat and another fraction to accelerated particles. We assume that the power-law exponent for the accelerated particles is the same throughout the jet volume, but that the number density of relativistic particles scales as $K_{\rm e} \propto j'^2$.

However, we cannot be certain that the dissipation rate of the magnetic field is proportional to j'^2. Therefore, we consider another prescription for the number density of emitting particles in the comoving frame, $K_{\rm e} \propto B'^2$. This corresponds to the condition of minimizing the sum of the energy densities of the magnetic field and relativistic particles, frequently used to obtain estimates of physical conditions in radio sources (e.g. Burbidge 1956; Pacholczyk 1970; Kronberg et al. 2001). In our case of strongly magnetized jets, the energy of the relativistic particles should be much smaller than the energy of the magnetic fields, but it may still be reasonable to assume that the particle energy density is proportional to B'^2.

4.1 Diffuse pinch

The non-relativistic force-free diffuse pinch is given by

$$B_\phi^{\rm nr} = \frac{ar}{1+(ar)^2} B_0, \quad B_z^{\rm nr} = \frac{1}{1+(ar)^2} B_0. \tag{23}$$

To calculate the polarization properties of such a jet, we can perform the integration of the Stokes parameters (2) and calculate the degree of polarization Π for the whole jet in a frame comoving with the jet, then use equations (19) to express Π as a function of the viewing angle in the laboratory reference frame. Alternatively, we can find the jet structure in the observer's frame, use relations (8) to calculate the polarization

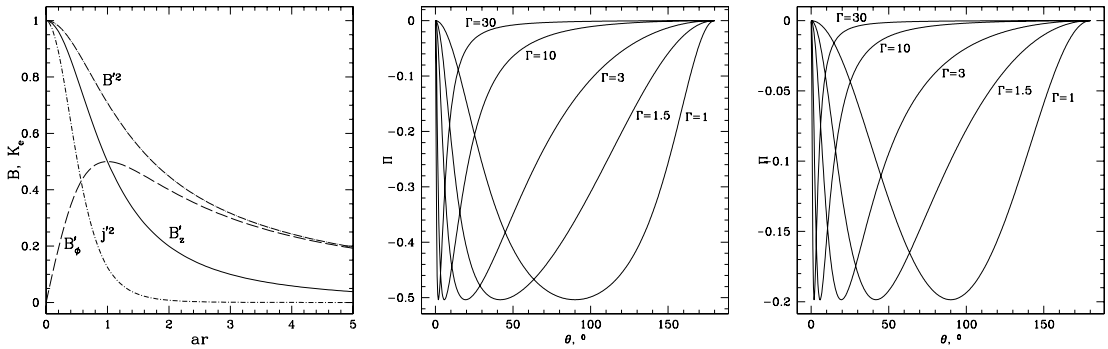

Figure 11. Polarization for a diffuse pinch, Section 4.1. (a) Radial profiles of B'_z, B'_ϕ, B'^2, and j'^2 (equations 24–25). Units are arbitrary: the profile of B_z is normalized to unity, the units of B_z and B_ϕ are the same, the profiles of the densities of emitting particles, B'^2 and j'^2, are also normalized to unity. (b) Degree of polarization for $p = 2.4$ for the density of relativistic particles $K_e \propto j'^2$, as a function of the observer angle θ for different bulk Lorentz factors Γ. (c) Same as (b), but for $K_e \propto B'^2$.

vector in the observer's frame and perform the integration of the Stokes parameters (2) in the observer's frame. The equivalence of the results of both calculations provides a consistency check.

The diffuse pinch configuration can be generalized to the relativistic case using the procedure described in Appendix B. The Lorentz transformation along the z-axis will lead to a radial electric field and distributed charge densities (if a non-relativistic pinch had a line current, a line charge would also appear in the relativistic case). First, we consider jets with $\Gamma =$ constant. The fields in the laboratory frame are then

$$B_z = \frac{B_0}{1+(ar)^2}, \quad B_\phi = \frac{ar\Gamma B_0}{1+(ar)^2}, \quad E_r = \sqrt{\Gamma^2-1}\,\frac{arB_0}{1+(ar)^2}. \tag{24}$$

The corresponding current density in the frame comoving with the plasma element is

$$j'_z = \frac{aB_0}{2\pi(1+a^2r^2)^2}, \quad j'_\phi = \frac{a^2B_0 r}{2\pi(1+a^2r^2)^2}, \quad j'^2 = \frac{a^2B_0^2}{4\pi^2(1+a^2r^2)^3}. \tag{25}$$

The diffuse pinch has a logarithmically divergent total poloidal flux $\Phi_z = \ln[1+(ar)^2]\ B_0\ \pi/a^2$, a pitch angle that increases with radius, $B_\phi/B_z = \Gamma ar$, and a total poloidal current $I_0 = B_0\Gamma/(2\ a)$.

We integrated this expression from $r = 0$ to large radii, $r \gg 1/a$, for two cases: when the number density of particles is $K_e \propto j'^2$ and $K_e \propto B'^2$. The results are presented in Fig. 11. The polarization vector is always perpendicular to the jet axis. The degree of polarization is large, especially in the case $K_e \propto j'^2$. Current density profile is more centrally peaked than the magnetic energy density profile (see Fig. 11a). This causes the emissivity to come primarily from the central jet region where the magnetic field is poloidally dominated in the frame comoving with the jet. In turn, this results in large perpendicular polarization. The perpendicular polarization increases with the concentration of the emissivity profiles toward the central axis.

4.2 Jets with reverse-field pinch and zero poloidal flux

Next we calculate the polarization from a jet with zero total poloidal flux, $\int_0^\infty B_z r\,\mathrm{d}r = 0$. This case corresponds to a large-scale magnetic field at the base of the jet generated by the disc itself, as opposed to the case of non-vanishing poloidal flux of an advected magnetic field. The following choice of force-free magnetic field (in the laboratory frame) is representative of the case with vanishing total flux:

$$B_z^{\rm nr} = B_0\frac{1-a^2r^2}{(1+a^2r^2)^3}, \quad B_\phi^{\rm nr} = B_0\Gamma\frac{ar\sqrt{2/15}}{(1+a^2r^2)^3}\sqrt{30+10a^2r^2+15a^4r^4+6a^6r^6+a^8r^8} \tag{26}$$

(see Fig. 12). We have the following expressions for the components of the current:

$$j'_\phi = \frac{cB_0}{4\pi}4a^2r\frac{2-a^2r^2}{(1+a^2r^2)^4}, \tag{27}$$

$$j'_z = \frac{cB_0}{4\pi}\frac{2\sqrt{30}a(a^2r^2-1)(a^2r^2-2)}{(1+a^2r^2)^4\sqrt{30+10a^2r^2+15a^4r^4+6a^6r^6+a^8r^8}}. \tag{28}$$

The results of the polarization calculations for the number density of particles $K_e \propto j'^2$ and $K_e \propto B'^2$ are presented in Fig. 12. Similar to the case of a diffuse pinch, the electric vector of the wave is orthogonal to the jet axis. The absolute value of the polarization degree is also large in the case of the reverse-field pinch, but only slightly less than in the case of the diffuse pinch. This is due to a somewhat larger ratio of the toroidal-to-poloidal field in the central regions of the reverse-field pinch. Similar to the case of the reverse-field pinch, the polarization degree for the $K_e \propto j'^2$ case is larger than the polarization degree for the $K_e \propto B'^2$ case.

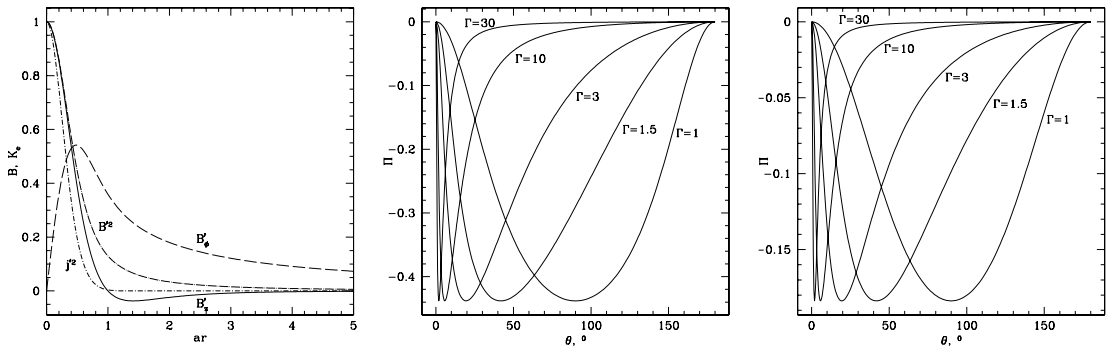

Figure 12. Polarization for a reverse-field pinch with vanishing total poloidal flux for the fields given by equations (26). Notations are the same as in Fig. 11. (a) Radial profiles. (b) Degree of polarization for $p = 2.4$ for the density of relativistic particles $K_e \propto j'^2$. (c) Degree of polarization for $p = 2.4$ for the density of relativistic particles $K_e \propto B'^2$.

4.3 Jets with multiple reversals of the axial magnetic field

As a further illustration, we consider the possibility that the axial magnetic field in the jet has multiple reversals. We also impose the condition that the total flux of the axial magnetic field vanishes, $\int_0^\infty B_z r\,\mathrm{d}r = 0$. This situation may correspond to a magnetic field produced as a result of amplification by the magnetorotational instability (Balbus & Hawley 1991, 1998) or a magnetic dynamo (Pariev, Colgate & Finn 2004) operating in the accretion disc. The loops of magnetic field can rise above the accretion disc, reconnect, and form multiply reversed magnetic field structures carrying no total poloidal flux. We choose the following form of the axial magnetic field in the frame comoving with the jet:

$$B_z^{\rm nr} = B_0 \frac{\cos \lambda a r}{(1 + a^2 r^2)}, \tag{29}$$

where $\lambda = 0.879$ is chosen to satisfy the condition $\int_0^\infty B_z r\,\mathrm{d}r = 0$. $B_\phi^{\rm nr}$ is then found by numerically integrating the non-relativistic force-free equilibrium equation. $B_\phi^{\rm nr} \propto 1/r$ for $r \gg a$. The toroidal magnetic field and electric field in the laboratory frame can be calculated from equation (B4).The current density in the frame comoving with the jet is calculated as

$$j'_\phi = \frac{2a^2 r \cos(\lambda a r)}{(1 + a^2 r^2)^2} + \frac{\lambda a \sin(\lambda a r)}{1 + a^2 r^2}, \quad j'^2 = j'^2_\phi \left(1 + \frac{B_z^{nr2}}{B_\phi^{nr2}}\right). \tag{30}$$

The radial dependencies of the fields in the frame comoving with the jet, $B'_z(r)$, $B'_\phi(r)$, and the two prescriptions for the number density of emitting particles, $K_e \propto j'^2$ and $K_e \propto B'^2$, are shown in Fig. 13.

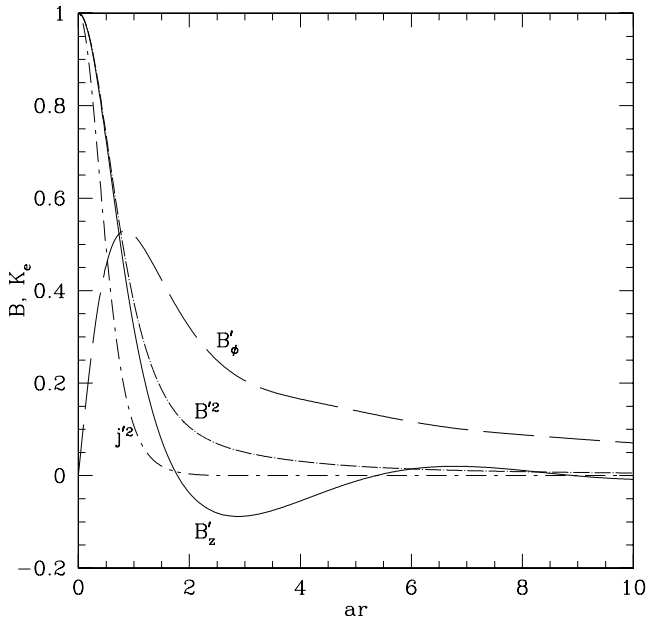

Figure 13. Radial profiles for a pinch with multiple axial field reversals for the fields given by equations (29)–(30).

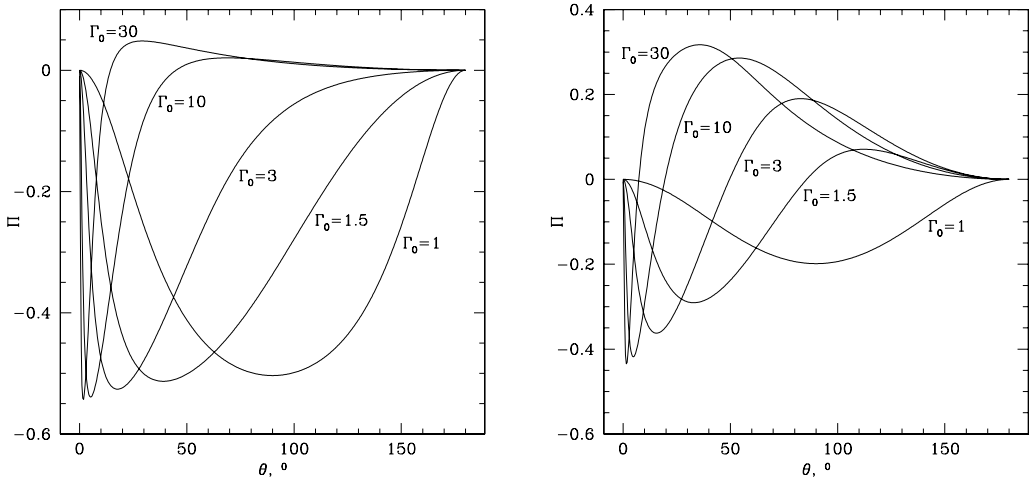

Figure 14. Polarization for the sheared diffuse pinch (for discussion see Section 5) for $p = 2.4$ integrated over the whole jet. (a) The density of relativistic particles $K_e \propto j'^2$. (b) The density of relativistic particles $K_e \propto B'^2$.

We perform the integration of the Stokes parameters for a constant emissivity from $r = 0$ to large radii, $r \gg 1/a$. The results for Π are almost identical with the polarization for the reverse-field pinch, Fig. 12. We do not plot these results in separate figures to save space. Therefore, the observation on Π made in the end of Section 4.2 are the same for the case of multiple reversals.

4.4 Emission from 'filled' jets without shear: conclusion

The three examples of jet profiles and two prescriptions for emissivity we have considered illustrate that the polarization remains perpendicular to the jet axis in all cases. Parallel polarization cannot be produced in models in which the energy density of the relativistic particles is $\propto j'^2$. In the case when the energy density of the emitting particles is $\propto B'^2$, the degree of polarization is small. The parallel polarization observed in some (many) sources cannot be explained using models in which the relativistic particles are distributed across the jet. The reason is that the current distribution and magnetic fields are highest on the axis, where the magnetic field in the jet rest frame is dominated by the poloidal field, so that the average emission is dominated by regions with large poloidal field. Thus, in order to produce parallel polarization *the emitting particles must be concentrated in the regions of stronger toroidal field*, closer to the edges of the jet.[3]

The results of this section indicate the possibility that *particle acceleration occurs selectively in the bulk of the jet, not too close to the axis* as we further argue in Section 6. Another possibility is strongly sheared jets, in which the emission from the central parts (which are dominated by poloidal magnetic field in the comoving frame) is beamed away from us. We investigate this possibility next.

5 EMISSION FROM SHEARED JETS

The jets considered in the previous section were all non-sheared, so that the degree of polarization can be derived in their rest frame and then the viewing angle transformed using the light-aberration formulae. In this section, we consider sheared jets when the axial bulk velocity is a function of radius in the jet. In this case, there is no reference frame in which the entire jet is at rest. The fully relativistic approach for calculating the Stokes parameters for an arbitrarily moving medium described in Section 2 is needed. As a model problem, we assume that the jet internal structure corresponds to a diffuse pinch (Section 4.1). In addition, we chose the following scaling of the Lorentz factor with radius:

$$\Gamma = 1 + \frac{1}{1 + (ar)^2}(\Gamma_0 - 1), \tag{31}$$

so that the axis of the jet moves with Lorenz factor Γ_0. Then, we follow the procedure for constructing the equilibrium of a relativistic force-free jet given in Appendix B.

As in Section 4, we investigate two example cases for the energy density of the relativistic emitting particles: $K_e \propto \boldsymbol{j}'^2$ and $K_e \propto B'^2$ (Fig. 14). Since there is no global reference frame in which the whole jet is at rest, the current density in the local comoving frame $\boldsymbol{j}'$ is now, in general, not equal to the curl of $\boldsymbol{B}^{nr}$. To calculate $\boldsymbol{j}'$, we first calculate the current density $\boldsymbol{j} = \nabla \times \boldsymbol{B}/(4\pi)$ and charge density $\rho_e = \nabla \times \boldsymbol{E}/(4\pi)$ in the laboratory frame. Then, we make a Lorentz transformation of the current four-vector to the local comoving frame of the plasma

[3] More precisely, the emission-weighted average pitch angle in the jet rest frame must not be small. In the case of force-free jets, this can only occur not too close to the jet axis.

element to obtain $\boldsymbol{j}'$. The result is that still $\boldsymbol{j}' = \nabla \times \boldsymbol{B}^{\rm nr}/(4\pi)$, i.e. terms containing $\mathrm{d}\Gamma/\mathrm{d}r$ cancel out in the expression for $\boldsymbol{j}'$. The reason for this cancellation is that the radial force balance is not broken by the introduction of the shear in the axial flow in the jet (see Appendix B).

At small viewing angles $\theta \leqslant 1/\Gamma_0$, the emission is dominated by the central regions, where the magnetic field in the rest frame of the moving plasma is mostly poloidal, so the polarization is perpendicular to the jet axis. At larger viewing angles $\theta \geqslant 1/\Gamma_0$, the emission from the central parts of the jet is beamed away, so that the average polarization may be along the jet.

6 ELECTROMAGNETICALLY DOMINATED JETS

In this paper, we present polarization calculations that indicate that large-scale magnetic fields may be responsible for the polarization observed in parsec-scale jets in AGNs. In order to produce the substantial degrees of polarization that are observed in these jets, the total energy density of the ordered component of the magnetic field must be at least comparable to the random component. This raises the question of how strong the magnetic fields in AGN jets can be. To quantify the dynamical importance of large-scale magnetic fields, it is useful to introduce the magnetization parameter σ as the ratio of the Poynting $F_{\rm Poynting}$ to the (cold) particle $F_{\rm p}$ fluxes:

$$\sigma = \frac{F_{\rm Poynting}}{F_{\rm p}} = \frac{B^2}{4\pi\Gamma\rho c^2} \approx \frac{B'^2}{8\pi\rho' c^2}, \tag{32}$$

where ρ and ρ' are plasma densities in the lab and jet frames. In hydrodynamical jets, $\sigma \ll 1$; MHD jets have $\sigma \sim 1$; electromagnetic jets have $\sigma \gg 1$.

In this paper we argue that AGN jets carry considerably strong large-scale magnetic fields, so that σ cannot be too small, i.e. $\sigma \geqslant 1$. Below we discuss the possibility that the energy is transported along the jets mainly in the form of the Poynting flux (so that $\sigma \gg 1$). It may be possible to overcome the difficulties of pure electron–positron beam models as well as ion-dominated models. Qualitatively, electromagnetic jets (or, rather, magnetic helices) will be toroidally dominated in the observer frame on parsec scales owing to conservation of the poloidal magnetic flux and poloidal current. As we have shown in this paper, this is consistent with observations. If a jet has a net poloidal current, the self-pinching of this current will tend to collimate it. In turn, the poloidal currents can become unstable to the excitation of anomalous resistivity and the subsequent development of resistive instabilities. The result will be the dissipation of poloidal currents or, equivalently, of the toroidal magnetic field. The dissipated energy can go primarily into the acceleration of electrons, similar to the case of solar flares. Thus, *a current that contributes to the jet collimation provides a natural source of energy for the re-energization of the jet via magnetic dissipation* (e.g. reconnection).

If the jets are magnetically dominated, the energy ultimately comes from the rotational energy of the central source (disc or black hole). It is first converted into magnetic energy by the dynamo action of the unipolar inductor (e.g. via the Blandford–Znajek mechanism), propagated in the form of a Poynting-flux-dominated flow and then dissipated by current instabilities at large distances from the sources.

Let us summarize the advantages of the magnetically dominated model for the energy transport in AGN jets (see also Blandford 2002; Lyutikov 2003).

(i) '**High quality**'. The energy stored in the low-entropy electromagnetic outflow has a 'high quality'. It can be efficiently converted into high-frequency electromagnetic radiation *far from the source*. For example, recent RHESSI and TRACE observations of the Sun indicate that the primary energy output in reconnection is in the form of *non-thermal electrons*, and only a small fraction goes into heating and bulk motion (Benz & Saint-Hilaire 2003).

(ii) **Variability**. Recent observations of high-energy emission from blazars with very short variability time-scales (as short as 20 minutes in Mrk 421 – Gaidos et al. 1996; Cui 2004) have stressed again the need for *in-situ* acceleration, since the synchrotron cooling times for the X-ray and especially γ-ray emitting electrons are an order of magnitude shorter than the light travel time from the core (and often shorter than the light crossing time of the emitting region itself).

Magnetic fields are strongly non-linear systems: slow evolution during which magnetic stresses build up can lead to the accumulation of a large amount of free energy, which is released in explosive events on a short time-scale (of the order of the Alfvén time-scale) as the system crosses the stability threshold. Such events happening in the central engine, close to the black hole and accretion disc, could be the source of flaring events that result in the emergence of new bright knots. Small-scale reconnection events could produce quasi-steady high-energy emission, analogous to the micro-flare paradigm for the quiescent emission of the solar corona (e.g. Benz & Krucker 1998; Krucker & Benz 2000). In addition, variations in the surrounding medium may lead to restructuring of the jet, accompanied by dissipation (Choudhuri & Konigl 1986). The magnetic field dissipation can be internal, and does not necessarily lead to the global disruption of the system, as happens, for example, in sawtooth oscillations in TOKAMAKs (e.g. Kadomtsev 1975). Current-driven instabilities in jets may proceed in a similar way (Appl et al. 2000).

(iii) **Particle acceleration**. In the case of an ordered spiral magnetic field, relativistic particles are restricted from moving in the radial direction – only radial drift motions due to perturbations of magnetic and electric fields, and scattering due to interaction with waves, could displace particles in the radial direction. Such radial motion of relativistic particles is very slow, so that they lose their relativistic energies by emitting synchrotron. Therefore, the synchrotron emitting particles can move only along the magnetic surfaces (roughly cylinders with constant radii, in our approximation). As we saw in Section 4, the existence of longitudinal polarization not too close to the axis of the jet is strongly suggestive of the hollow synchrotron emissivity profile across the jet, when the maximum of the emissivity and relativistic particles number density is reached at the jet periphery. As such, particles must be either ejected from the central engine or produced locally at the

periphery of the jet. The former case cannot account for the centimetre radio emission of parsec jets, because the synchrotron cooling time for the particles is shorter than the time it takes light to reach parsec scales starting from the central engine (this was pointed out a while ago, e.g. Begelman et al. 1984). Thus, we are left with the latter possibility and the need for a mechanism to energize the particles *in situ*.

Dissipation of the magnetic field leads to particle acceleration that produces a power-law distribution of accelerated particles, as is exemplified by solar magnetic dissipation (with reconnection being the prime example) is highly uncertain: it depends critically on the kinetic and geometric properties of the plasma, which are very hard to measure observationally. This situation can be contrasted with shock acceleration schemes, where a qualitatively correct result for the spectrum of accelerated particles (a kinetic property!) can be derived from simple *macroscopic* considerations.

In spite of these difficulties, acceleration (or pre-acceleration) of electrons in some type of reconnection layer may provide an alternative possibility (or the first stage) for shock acceleration. First, we know that it works on the Sun. Secondly, magnetic dissipation can accelerate particles from a thermal bath, without the need for pre-acceleration. (Recall that only electrons with $\gamma_e \geqslant \Gamma_s m_p/m_e$ can be accelerated at a relativistic shock; here Γ_s is the shock Lorentz factor, and m_p and m_e are the proton and electron masses.) Thirdly, acceleration in reconnection layers can produce very-hard power-law spectra, $dn/d\gamma \sim \gamma^{-1}$ (Hoshino 2002; Larrabee et al. 2003). The fact that reconnection models can produce spectra that are prohibitively hard for shock acceleration can serve as a distinctive property of electromagnetic models.

(iv) **Large-scale stability and small-scale dissipation**. Relativistic electromagnetic jets are expected to be less susceptible to instabilities due to interaction with the external medium, as well as internal instabilities. In the case of interactions with an external medium, the magnetic field has a stabilizing effect on the surface modes, especially if there is longitude shear and rotation of the jet (Istomin & Pariev 1994, 1996). Kelvin–Helmholtz instability on the boundary between a moving force-free jet and the ambient gas is suppressed because of the very large expected density contrast between inside and outside of the jet (e.g. Hardee 1979). Rigorous investigation of the 'current driven' instability for the electromagnetic field configurations that we consider has not been done, and our remarks on the possible large-scale stability of such a jet are of a speculative nature. On the other hand, the presence of velocity shear would lead to the formation of critical layers where dissipative effects become important (Pariev et al. 2003). Thus, rotation and shear can lead to large-scale stabilization and small-scale de-stabilization of the jet. The energy released owing to small-scale dissipation could be used to power the jet luminosity.

(v) **Knots**. AGN jets have distinct structures along the jets in the form of knots, fainter bridges of emission, etc. These structures could be regions of enhanced dissipation, in which case they are likely to break cylindrical and/or translational symmetry along the jet; alternatively, they could be the jet structures that emit preferentially in our direction. Quasi-periodic bright knots are observed in the jets of many AGNs, such as M87 (Marshall et al. 2002), 3C273 (Marshall et al. 2001) and 4C 19.44/1354+195 (Sambruna et al. 2002). An intriguing possibility is that the quasi-periodic bright knots are associated with large-amplitude waves propagating in the jet (Istomin & Pariev 1996; Pariev et al. 2003). These waves can be excited by explosive reconnection events at the base of the jet. Alternatively, accretion disc instabilities and the evacuation and reformation of parts of an accretion disc could be the source of these large-amplitude waves (Lovelace, Romanova & Newman 1994; Lovelace et al. 1997). The propagation of such waves in a radially inhomogeneous jet can be weakly dissipative, providing a means of energizing particles in the jet (Beresnyak, Istomin & Pariev 2003).

At present, hydrodynamical models of AGN jets are much better developed (e.g. Hardee 2003). It remains to be seen if electromagnetic jets are able to reproduce equally well the large-scale dynamical behaviour. In addition, radiation modelling of AGN spectra allowing for a two-zone structure of the magnetic field (low inside the acceleration region, high in the bulk) needs to be done.

7 DISCUSSION AND CONCLUSIONS

We have analysed the polarization properties of the synchrotron emission of relativistic cylindrical jets with helical magnetic fields, taking into account the relativistic motion of the jet. We considered uniform radial profiles of the velocity of the jet as well as sheared velocity profiles in which the velocity is higher at the centre of the jet and decreases to zero at the outer boundary of the jet. We have explored a number of fairly general magnetic-field structures and emission profiles, on which we base the following conclusions.

(1) We stress again that, in the case of relativistically moving optically thin jets, the observed direction of the polarization *is not generally orthogonal* to the projected direction of the magnetic field. We accordingly encourage observers always to plot the direction of the electric field of the wave, not the 'inferred direction of the magnetic field'. It is important to employ a correct Lorentz transformation of the polarization, regardless of the model considered: calculations of the polarization from internal shocks must take this effect into account as well. To infer the structure of the magnetic field from the observed polarization map, one needs to know the structure of the velocity field as well. Fortunately, for the case of AGN jets one can make reasonable assumptions about the structure of the velocity field (e.g. axisymmetry), which together with spacial averaging still allows one to derive conclusions about the field structure.

(2) To produce polarization along the jet axis, the emissivity-weighted pitch angle of the magnetic field in the jet frame cannot be small. This can be achieved either (i) if a jet has a pinch configuration with no, one or many reversals *and* the jet emissivity is confined to a narrow region of radii where the toroidal magnetic field is of the order of the poloidal field in the jet frame, or (ii) if the velocity of the jet changes with radius such that the relativistic beaming is maximum in a narrow range of radii closer to the outer boundary of the jet, where the toroidal magnetic field is of the order of the poloidal field in the jet frame.

(3) The polarization electric vector position angle (EVPA) integrated over the jet cross section shows a bimodal distribution, being directed either along or orthogonal to the jet, in accordance with observations (Cawthorne et al. 1993; Gabuzda et al. 2000).

(4) Strongly beamed jets (viewed at $\theta \leqslant 1/\Gamma$) can have polarization directed along the jet axis only if the toroidal magnetic field strongly dominates over the poloidal field in the observer's frame, $B_\phi/B_z \geqslant \Gamma \gg 1$. This will be true if the toroidal field is at least comparable to the poloidal field in the jet frame. In this case, we have in the jet frame $B'_\phi \sim B'_z$, so that the jet is expected to be dynamically stable to pinches and kinks. When an orthogonal jump of the polarization position angle is seen along such jets, we can estimate $B_\phi/B_z \sim \Gamma \gg 1$. The occurrence of orthogonal jumps of polarization should be more prominent in sources with flatter spectra.

(5) In resolved jets, the asymmetry of the polarization profile perpendicular to the jet axis (e.g. as determined by the intensity profile) can be used to determine whether the spin axis of the central object is aligned or anti-aligned with the jet axis.

(6) In a resolved cylindrical shell with $B'_\phi \sim B'_z$, the polarization in the central parts is along the jet, while the polarization at the jet edges is orthogonal to the jet axis, in accordance with observations (Attridge et al. 1999; Pushkarev & Gabuzda 2002; Pushkarev et al. 2005). This provides further evidence that the jet emissivity is confined to a narrow region of radii at the periphery of the jet, where the toroidal magnetic field is of the order of the poloidal field in the jet frame.

These results support the possibility that the characteristic behaviour of the polarization of AGN jets arises precisely because these jets carry helical magnetic fields. Additional support for this scenario comes from the observations of differential Faraday rotation across the jets of BL Lac objects, which can be understood as a natural consequence of a toroidal or helical magnetic-field configuration (Gabuzda et al. 2004), and the evidence that the circular polarization of AGN cores displays a constant sign over long intervals (Homan, Attridge & Wardle 2001). Both of these last two effects argue in favour of the dominant role of large-scale magnetic fields in the jets. It is likewise not difficult to account for possible exceptions to the general tendencies stated above. For example a non-axisymmetric structure of the jet can give rise to a relative orientation of the EVPA relative to the jet that differs from 0° or 90° (there are theoretical grounds for non-axisymmetric jets – see Choudhuri & Konigl 1986). The curved jet in Fig. 1 may be viewed close to its axis, so that it may be represented by two quasi-cylindrical pieces smoothly changing direction at a merger point. Then, the resolved and unresolved EVPA will be approximately aligned with the axis of the cylindrical pieces because of the bimodality described above. The largest deviation of the EVPA from such alignment is expected to happen at the point of jet bending. This is indeed the case for the EVPA plotted on Fig. 1: at the location of the bend, the EVPA makes an angle of almost 45° with the local direction of the middle axis of the brightness distribution there.

The conditions for having appreciable longitudinal polarization in a relativistic jet are more restrictive than those for orthogonal polarization. This is a purely geometrical effect. For a given jet structure, the highest degree of longitudinal polarization will be observed when the jet is viewed at the angle $\theta \sim 1/\Gamma$. In this case, the line of sight is orthogonal to the jet axis in the jet rest frame. It is thought that, statistically, $\theta \sim 1/\Gamma$ for the pc-scale jets of core-dominated AGN, while most kpc-scale jets are viewed at angles $\theta \gg 1/\Gamma$ in the observer's rest frame, so that the line of sight makes a small angle with the jet axis in the comoving frame. Therefore, the observed kpc-scale jets should have orthogonal polarization more frequently than pc-scale jets. This stresses again that, *owing to relativistic kinematic effects, it is not possible to draw a firm conclusion about whether a jet is dominated by toroidal or poloidal fields based purely on the observed direction of polarization.*

Another implication of our calculations is that the polarization properties of an intrinsically similar jet and counter-jet can be very different (if the counter-jet is detected), owing to the different angles that the line of sight makes with the jet magnetic field in the two cases. It follows from Fig. 7 that, in the counter-jet, high degrees of polarization, $\geqslant$10 per cent, can be directed only orthogonal to the jet axis, while low degrees of polarization can be either longitudinal or orthogonal. In the strongly relativistic limit $\Gamma \gg 1$, jets viewed at angles $\theta = C/\Gamma$ and $\theta_{\rm ob} = 1/(\Gamma\ C)$, where C is some constant, $C \ll \Gamma$, should have the same linear polarization properties (in this case, the lines of sight make the same angles with the jet axis in the jet rest frame).

The typical degrees of polarization observed in compact AGNs are fairly low, of the order of a few to 10 or 15 per cent. Modest polarization is observed from any jet that has comparable toroidal and poloidal fields in the jet rest frame, $B'_\phi \sim B'_z$. (Such relatively weakly polarized relativistic jets are still strongly toroidally dominated in the observer's frame.) The condition $B'_\phi \sim B'_z$ can be reached self-consistently: over-expansion of a jet would lead to an increase of the ratio B'_ϕ/B'_z, making the jet more likely to be unstable. The development of instabilities would lead to the dissipation of poloidal current and a decrease in B'_ϕ/B'_z (Colgate & Li 1998). Calculations of relativistic force-free expanding helices produced by the twisting of the magnetic field lines by the accretion disc also indicate that $B'_\phi \sim B'_z$ in the inner collimated part of the expanding magnetic helix (Lovelace et al. 2002). Thus, if the modest observed degrees of polarization are indeed due to the presence of comparable toroidal and poloidal fields in the jet frame, this would imply that *all relativistic jets are dominated by the toroidal magnetic field component in the observer's frame*.

Toroidally dominated jets are also expected on theoretical grounds. Suppose that AGN jets are launched from a black-hole–disc system with large-scale poloidal and toroidal fields at the surface of the disc. During the acceleration of the flow by magnetic stresses, the flow expands so that the ratio of B_ϕ to B_z will increase approximately linearly with cylindrical radius. If the jets are toroidally dominated on a cylindrical scale $\varpi \sim 0.3$ pc with $B_\phi/B_z \sim \Gamma \sim 10$, this implies that the Alfvén point (where $B_\phi/B_z \sim 1$) is located at $\varpi \sim 10^{17}$ cm, so that the ratio of the fields is $B_\phi/B_z \sim 0.1$ at the outer edge of the disc, located at $\varpi \sim 500\,R_G \sim 10^{16}$ cm ($R_G \sim 3 \times 10^{13}$ cm is the Schwarzschild radius of the supermassive black hole). Further in, the pinch angle depends on the details of the EMF distribution in the disc (e.g. Blandford 1976). This helps to reconcile the strong toroidal dominance in the jets expected on theoretical grounds with the observed EVPA orthogonal to the jet axis.

In this paper, we have considered jets that have achieved asymptotic cylindrical collimation. Close to the central object, the jets are often observed to be conically divergent. Though a separate set of calculations for conical jets are necessary, qualitatively, we expect that the ratio of the toroidal and poloidal fields increases with distance, so that the jets are likely to have polarization along the jet axis at larger distances.

This type of behaviour (predominance of longitudinal polarization at larger distances) is seen in some cases (Denn et al. 2000; Gabuzda & Gómez 2001).

ACKNOWLEDGMENTS

VP acknowledges partial support from DOE grant DE-FG02-00ER54600 and support from the Center for Magnetic Self-Organization in Laboratory and Astrophysical Plasmas funded by the National Science Foundation.

REFERENCES

Appl S., Camenzind M., 1992, 256, 354
Appl S., Camenzind M., 1993, A&A, 274, 699
Appl S., Lery T., Baty H., 2000, A&A, 355, 818
Attridge J. M., Roberts D. H., Wardle J. F. C., 1999, ApJ, 518, 87
Balbus S. A., Hawley J. F., 1991, ApJ, 376, 214
Balbus S. A., Hawley J. F., 1998, Rev. Mod. Phys., 70, 1
Beckert T., 2003, Ap&SS, 288, 123
Beckert T., Falcke H., 2002, A&A, 388, 1106
Begelman M. C., Blandford R. D., Rees M. J., 1984, Rev. Mod. Phys., 56, 255
Benz A. O., Krucker S., 1998, Solar Phys., 182, 349
Benz A. O., Saint-Hilaire P., 2003, astro-ph/0308321
Beresnyak A. R., Istomin Ya. N., Pariev V. I., 2003, A&A, 403, 793
Biretta J. A., Owen F. N., Hardee P. E., 1983, ApJ, 274, 27
Bjornsson C.-I., 1982, ApJ, 260, 855
Blandford R. D., 1976, MNRAS, 176, 465
Blandford R. D. 2002, in Sunyaev R., ed., Lighthouses of the Universe: the Most Luminous Celestial Objects and Their Use for Cosmology. Springer-Verlag, Berlin, p. 381
Blandford R. D., Pringle J. E., 1976, MNRAS, 176, 443
Blandford R. D., Znajek R. L., 1977, MNRAS, 179, 433
Blandford R. D., Königl A., 1979, ApJ, 232, 34
Blandford R. D., Payne D. G., 1982, MNRAS, 199, 883
Bodo G., Mignone A., Rosner R., 2004, Phys. Rev. E, 70, 036304
Burbidge G. R., 1956, ApJ, 124, 416
Camenzind M., 1995, Rev. Mod. Astron., 8, 201
Cawthorne T. V., Wardle J. F. C., Roberts D. H., Gabuzda D. C., 1993, ApJ, 416, 519
Choudhuri A. R., Konigl A., 1986, ApJ, 310, 96
Clarke D. A., Burns J. O., Feigelson E. D., 1986, ApJ, 300, 41
Cocke W. J., Holm D. A., 1972, Nature Phys. Sci., 240, 161
Colgate S. A., Li H., 1998, Ap&SS, 264, 357
Contopoulos J., Lovelace R. V. E., 1994, ApJ, 429, 139
Cui W., 2004, ApJ, 605, 662
Denn G. R., Mutel R. L., Marscher A. P., 2000, ApJs, 129, 61
Gabuzda D. C., 2003, New Astron. Rev., 47, 599
Gabuzda D. C., Chernetskii V. A., 2003, MNRAS, 339, 669
Gabuzda D. C., Gómez J. L., 2001, MNRAS, 320, L49
Gabuzda D. C., Mullan C. M., Cawthorne T. V., Wardle J. F. C., Roberts D. H., 1994, ApJ, 435, 140
Gabuzda D. C., Pushkarev A. B., Cawthorne T. V., 2000, MNRAS, 319, 1109
Gabuzda D. C., Pushkarev A. B., Garnich N. N., 2001a, MNRAS, 327, 1
Gabuzda D. C., Gómez J. L., Aguda I., 2001b, MNRAS, 328, 719
Gabuzda D. C., Murray E., Cronin P., 2004, MNRAS, 351, L89
Gaidos J. A. et al., 1996, Nat, 383, 319
Ginzburg V. L., 1989, Applications of Electrodynamics in Theoretical Physics and Astrophysics. Gordon & Breach, New York
Hardee P. E., 1979, ApJ, 234, 47
Hardee P. E., 2003, ApJ, 597, 798
Heyvaerts J., Norman C., 1989, ApJ, 347, 1055
Heyvaerts J., Norman C., 2003, ApJ, 596, 1240
Hoshino M., 2002, in Nakajima K., Deguchi M., eds, AIP Conf. Proc. 634, Direct Particle Acceleration in Astroplasmas. Am. Inst. Phys., New York, p. 169
Hughes P. A., Aller H. D., Aller M. F., 1989a, ApJ, 341, 54
Hughes P. A., Aller H. D., Aller M. F., 1989b, ApJ, 341, 68
Homan D. C., Attridge J. M., Wardle J. F. C., 2001, ApJ, 556, 113
Istomin Ya. N., Pariev V. I., 1994, MNRAS, 267, 629
Istomin Ya. N., Pariev V. I., 1996, MNRAS, 281, 1
Kadomtsev B. B., 1975, Soviet J. Plasma Phys., 1, 710
Kigure H., Uchida Y., Nakamura M., Hirose S., Cameron R., 2004, ApJ, 608, 119
Komissarov S. S., 2002, MNRAS, 336, 759
Konigl A., Choudhuri A. R., 1985, ApJ, 289, 188
Kronberg P. P., Dufton Q. W., Li H., Colgate S. A., 2001, ApJ, 560, 178

Krucker S., Benz A. O., 2000, Solar Phys., 191, 341
Laing R. A., 1980, MNRAS, 193, 439
Laing R. A., 1981, ApJ, 248, 1981
Larrabee D. A., Lovelace R. V. E., Romanova M. M., 2003, ApJ, 586, 72
Li H., Lovelace R. V. E., Finn J. M., Colgate S. A., 2001, ApJ, 561, 915
Lovelace R. V. E., Romanova M. M., 2003, ApJ, 596, L159
Lovelace R. V. E., Romanova M. M., Newman W. I., 1994, ApJ, 437, 136
Lovelace R. V. E., Newman W. I., Romanova M. M., 1997, ApJ, 484, 628
Lovelace R. V. E., Li H., Koldoba A. V., Ustyugova G. V., Romanova M. M., 2002, ApJ, 572, 445
Lynden-Bell D., 1996, MNRAS, 279, 389
Lynden-Bell D., 2003, MNRAS, 341, 1360
Lyubarskii Yu. E., 1999, MNRAS, 308, 1006
Lyutikov M., 2003, New Astron. Rev., 47, 513
Lyutikov M., Blandford R., 2003, astro-ph/0312347
Lyutikov M., Uzdensky D., 2003, ApJ, 589, 893
Lyutikov M., Pariev V. I., Blandford R. D., 2003, ApJ, 597, 998
Marscher A. P., Jorstad S. G., Mattox J. R., Wehrle A. E., 2002, ApJ, 577, 85
Marshall H. L. et al., 2001, ApJ, 549, L167
Marshall H. L., Miller B. P., Davis D. S., Perlman E. S., Wise M., Canizares C. R., Harris D. E., 2002, ApJ, 564, 683
Michel F. C., 1973, ApJ, 180, 207
Moellenbrock G. A., Roberts D. H., Wardle J. F. C., 2000, in Hirabayashi H., Edwards P. G., Murphy D. W., eds, Proc. VSOP Symp., Astrophysical Phenomena Revealed by Space VLBI. Inst. Space Astronaut. Sci., Sagamihara, p. 129
Nakamura M., Uchida Y., Hirose S., 2001, New Astron., 6, 61
Owen F. N., Hardee P. E., Cornwell T. J., 1989, ApJ, 340, 698
Pacholczyk A. G., 1970, Radio Astrophysics. Freeman and Co., San Francisco
Pariev V. I., Istomin Ya. N., Beresnyak A. R., 2003, A&A, 403, 805
Pariev V. I., Colgate S. A., Finn J. M., 2004, ApJ, submitted
Pushkarev A. B., Gabuzda D. C., 2002, in Laing R., Blundell K., eds, ASP Conf. Ser. 250, Particles and Fields in Radio Galaxies. Astron. Soc. Pac., San Francisco, p. 200
Pushkarev A. B., Gabuzda D. C., Vetukhnovskaya Yu. N., Yakimov V. E., 2005, MNRAS, 356, 859
Ruszkowski M., 2003, Ap&SS, 288, 133
Sambruna R., Maraschi L., Tavecchio F., Urry C. M., Cheung C. C., Chartas G., Scarpa R., Gambill J. K., 2002, ApJ, 571, 206
Sauty C., Tsinganos K., Trussoni E., 2002, Lecture Notes in Physics, 589, 41
Sazonov V. N., 1969, AZh, 46, 502
Tomimatsu A., Matsuoka T., Takahashi M., 2001, Phys. Rev. D, 64, 123003
Torricelli-Ciamponi G., Pietrini P., 1990, ApJ, 361, 32
Turland B. D., Scheuer P. A. G., 1976, MNRAS, 176, 421
Uchida T., 1997, Phys. Rev. E, 56, 2181
Ustyugova G. V., Lovelace R. V. E., Romanova M. M., Li H., Colgate S. A., 2000, ApJ, L21
Zhelezniakov V. V., 1996, Radiation in Astrophysical Plasmas. Kluwer, Dordrecht
Zheleznyakov V. V., Koryagin S. A., 2002, Astron. Lett., 28, 727

APPENDIX A: COMPARISON WITH BLANDFORD & KÖNIGL (1979)

For comparison with previous calculations (Blandford & Königl 1979), we adopt a frame aligned with the direction of motion. In this frame (quantities measured in this frame are labelled with the subscript BK),

$$\left.\begin{aligned} \boldsymbol{B}_{\rm BK} &= \{\cos\eta_{\rm BK}\sin\psi'_{\rm BK}, -\sin\eta_{\rm BK}, \cos\eta_{\rm BK}\cos\psi'_{\rm BK}\} \\ \hat{\boldsymbol{n}} &= \{\cos\theta_{\rm BK}, 0, \sin\theta_{\rm BK}\} \\ \boldsymbol{v} &= \beta\{1,0,0\} \\ \boldsymbol{e}_{\rm BK} &= \{-\cos\xi_{\rm BK}\sin\theta_{\rm BK}, \sin\xi_{\rm BK}, \cos\xi_{\rm BK}\cos\theta_{\rm BK}\}. \end{aligned}\right\} \tag{A1}$$

We find from equations (8) that

$$\tan\xi_{\rm BK} = \cot\eta_{\rm BK}\frac{\cos\left(\theta_{\rm BK}+\psi'_{\rm BK}\right)-\beta\cos\psi'_{\rm BK}}{1-\beta\cos\theta_{\rm BK}}, \tag{A2}$$

reproducing equation (16) in Blandford & Königl (1979). The angle between $\hat{\boldsymbol{B}}$ and $\hat{\boldsymbol{e}}$ is

$$\begin{aligned} \cos\zeta &= (\hat{\boldsymbol{B}}\times\hat{\boldsymbol{e}}) = \cos\eta_{\rm BK}\cos\xi_{\rm BK}\cos(\theta_{\rm BK}+\psi'_{\rm BK}) - \sin\eta_{\rm BK}\sin\xi_{\rm BK} \\ &= \frac{\beta\cos\eta_{\rm BK}\sin\theta_{\rm BK}\sin(\theta_{\rm BK}+\psi'_{\rm BK})}{\sqrt{(1-\beta\cos\theta_{\rm BK})^2+\cot^2\eta_{\rm BK}[\cos(\theta_{\rm BK}+\psi'_{\rm BK})-\beta\cos\psi'_{\rm BK}]^2}}. \end{aligned} \tag{A3}$$

APPENDIX B: RELATIVISTIC FORCE-FREE JETS

Conventionally, the structure of relativistic force-free jets has been considered in terms of the relativistic Grad–Shafranov equation, which for cylindrical geometry becomes a second-order ordinary differential equation (e.g. Appl & Camenzind 1993). Only few exact solutions have

been found (Appl & Camenzind 1993; Istomin & Pariev 1994). The structure of relativistic jets (pinches) is more complicated than that of non-relativistic jets. In addition to the poloidal and toroidal magnetic fields, a relativistic jet has a radial electric field, which can be of the same order of magnitude as the total magnetic field, and a charge density, which can approach $\rho_e \sim j/nec$ (so that the electric forces are comparable to the magnetic forces, $\rho_e E \sim jB$).

In a force-free approximation (Michel 1973; Uchida 1997; Komissarov 2002; Lyutikov & Blandford 2003), it is assumed that inertia and pressure forces are not important, so that the force balance is determined only by electromagnetic forces $\boldsymbol{E}\nabla\cdot\boldsymbol{E}/4\pi + \boldsymbol{j}\times\boldsymbol{B} = 0$. This, combined with Maxwell's equations and the ideal condition $\boldsymbol{E}\cdot\boldsymbol{B} = \boldsymbol{0}$, allows one to express the current in terms of the fields:

$$\boldsymbol{j} = \frac{(\boldsymbol{E}\times\boldsymbol{B})\nabla\cdot\boldsymbol{E} + (\boldsymbol{B}\cdot\nabla\times\boldsymbol{B} - \boldsymbol{E}\cdot\nabla\times\boldsymbol{E})\boldsymbol{B}}{4\pi B^2}. \tag{B1}$$

In addition, it is assumed that $B^2 - E^2 > 0$ (this ensures that there is a frame in which the electric field is zero). It is possible to define an electromagnetic velocity, which is equal to the plasma velocity across the magnetic field:

$$\beta_{\rm EM} = \frac{\boldsymbol{E}\times\boldsymbol{B}}{B^2}. \tag{B2}$$

The velocity along the magnetic field is not defined and can be chosen arbitrarily, subject to the physical constraint that the total velocity is lower that the speed of light.

For stationary cylindrical jets, the above relations imply that the non-zero components of the electromagnetic fields are B_ϕ, B_z and E_r, which are functions of r only. There is a charge density $\rho = \nabla\cdot\boldsymbol{E}/4\pi = \partial_r\,(rE_r)/4\pi\,r$ and current $\boldsymbol{j} = (1/4\pi)\,\nabla\times\boldsymbol{B}$. We find then that (Istomin & Pariev 1994)

$$B_z^2 = \frac{1}{2r}\partial_r r^2\left(B_z^2 + B_\phi^2 - E_r^2\right). \tag{B3}$$

This is an equation describing the equilibrium of a *relativistic* force-free jet. It reduces to the non-relativistic force-free equilibrium if $E_r = 0$. Next, we note that both sides of this equation are unchanged under a Lorentz boost along z ($B_z^2 + B_\phi^2 - E_r^2 = \boldsymbol{B}^2 - \boldsymbol{E}^2$ is a relativistic invariant and B_z does not change under a boost along z). If $|E_r(r)| < |B_\phi\,(r)|$, it is possible to choose the velocity of a radius-dependent Lorentz boost $\beta(r)$ such that the electric field will vanish. Then, the magnetic fields $B_\phi^{\rm nr}(r)$ and $B_z^{\rm nr}(r)$ in the frame where $E_r = 0$ will satisfy the non-relativistic force-free jet equilibrium. This implies that any solution for a *relativistic* force-free jet with $|E_r(r)| < |B_\phi\,(r)|$ can be obtained from a known solution for a non-relativistic pinch, $B_z^{\rm nr}(r)$ and $B_\phi^{\rm nr}(r)$, by making a *formal radius-dependent boost* along the z-axis:

$$E_r = \beta\Gamma B_\phi^{\rm nr}, \quad B_\phi = B_\phi^{\rm nr}\Gamma, \quad B_z = B_z^{\rm nr}, \tag{B4}$$

where $\beta \equiv \beta\,(r)$ and $\Gamma = 1/\sqrt{1-\beta^2}$. We stress that this transformation is not a physical Lorentz transformation – it can have a radius-dependent z-velocity, so that β and Γ are functions of r.

This method does not allow us to find solutions when $|E_r(r)| \geqslant |B_\phi\,(r)|$ (but $|E_r(r)| < |B(r)|$). In the latter case, there is no local frame where E_r would be zero. The equation (B3) can be integrated to give

$$\int_0^r r'^2\,\frac{{\rm d}B_z^2(r')}{{\rm d}r'}\,{\rm d}r' = r^2\left[E_r^2(r) - B_\phi^2(r)\right]. \tag{B5}$$

One can see that, if the poloidal magnetic field B_z is a monotonic decreasing function of radius, then $|E_r(r)| < |B_\phi\,(r)|$ for any r and such solutions can be obtained using the method described here. If ${\rm d}B_z^2/{\rm d}r \geqslant 0$ for some r, then our method may not find all solutions having such $B_z(r)$. On the contrary, any solution that cannot be obtained as a result of a formal Lorentz boosting of a non-relativistic force-free solution must have ${\rm d}B_z^2/{\rm d}r \geqslant 0$ in at least some interval of radii. An additional relativistic pinch solution can be obtained by adding a line charge $E_r \sim 1/r$. Although this provides intuitive physical insight into possible relativistic force-free configurations by relating them to the non-relativistic solutions, the radius-dependent Lorentz boost method allows us to obtain only a subclass of all possible relativistic solutions. Nevertheless, in this work we limit our analysis to solutions that can be obtained by this method and have $|E_r(r)| < |B_\phi\,(r)|$.

For cylindrical jets, the axial and azimuthal electromagnetic velocities are $\beta_{{\rm EM},z} = E_r B_\phi/B^2$ and $\beta_{{\rm EM},\phi} = -\,B_z E_r/B^2$. The plasma velocity along the magnetic field is not constrained by the force-free equations. In the previous sections, when calculating the emissivity and Doppler boosts we assumed that the total plasma velocity is along the z-axis and that there is no rotation. This implies that the emitting plasma indeed slides along the magnetic field in such a way as to make the azimuthal velocity equal to zero. This may not be true in real jets; then one needs to modify the relations allowing for radial-dependent axial and azimuthal velocities. An alternative possible choice of the velocity of the plasma could be one that minimizes the kinetic energy of the flow. In this case, the velocity of the plasma will be the electromagnetic velocity $\beta_{\rm EM}$, since the absolute value of the velocity cannot be smaller than the electromagnetic velocity. This choice for the velocity field of the plasma was used in the previous relativistic calculations of polarization from cylindrical relativistic force-free jets by Pariev et al. (2003). Since Pariev et al. (2003) also assumed that B_z is constant with radius, their field configuration cannot be obtained by the method described in this appendix.

This paper has been typeset from a TEX/LATEX file prepared by the author.